ELSEVIER

Journal of Molecular Structure (Theochem) 465 (1999) 33–67

THEO CHEM

A geometrical algorithm to search the conformational space (GASCOS) of flexible molecules

L.N. Santagata[a], F.D. Suvire[a], R.D. Enriz[a,*], L.L. Torday[b], I.G. Csizmadia[c]

[a]*Departamento de Química, Facultad de Química, Bioquímica y Farmacia, Universidad Nacional de San Luis, 5700 San Luis, Argentina*
[b]*Departament of Pharmacology and Pharmacotherapy, Albert Szent-György Medical University, H-6701 Szeged, Hungary.*
[c]*Lash Miller Chemical Laboratories, University of Toronto, Toronto, Ontario, Canada M5S 3H6*

Received 26 August 1998; accepted 25 September 1998

Abstract

We report a geometrical algorithm to search the conformational space (GASCOS), with the goal to evaluate, in a computationally effective way, all possible conformations of a flexible molecule. The present report itself consists of two parts. The first part is primarily devoted to the mathematical principles on which our approach is based. The basic principles are illustrated in terms of the conformational aspect of small normal hydrocarbons: C_nH_{2n+2}. In the second half of the paper we apply the geometrical approach to a set of specific chemical problems namely, partially fluorinated propanes are used in order to determine the steric requirement and, therefore, the spatial proximity of the terminal atoms during multiple internal rotations. In one type of application the torsion about the bond was regarded as a continuous variable by choosing the increment in torsional angle ($\Delta\theta$) to be small, such as 5°. In this approach we were able to assess the spatial requirement and therefore any possible collision of rotating moieties. In an other type of application $\Delta\theta$ was assumed to be as large as 120°, thus the internal rotational angle was regarded as a variable that can assume only discrete values (g^+, a, g^-). In this fashion, the program could generate an input file for empirical force field, semi-empirical MO or ab initio molecular computations within the framework of multidimensional conformational analysis (MDCA). In other words GASCOS could become the driver program for any energy calculating software. Finally, when an unusually short distance was obtained by the GASCOS method, it was then possible to consider such an occurrence as an indicator of a probable conformational catastrophe.

Keywords: Conformational space; Geometrical algorithm; Flexible molecules

1. Notation

In this paper we use the following notation:

1. Atoms denoted by capital letters; e.g. A, B, C, etc.
2. Directions are denoted by full arrows; e.g. $\overrightarrow{AB}$
3. Vectors are denoted with half arrows; e.g. $\vec{R}_A$, $\vec{R}_B$, $\vec{D}_{AB}$, etc.
4. Vectors $\vec{R}_A$ and $\vec{R}_B$ are with respect to arbitrary origin O, and vector $\vec{D}_{AB}$ is along the AB bond.
5. Unit vectors are denoted by a hat, e.g. $\hat{n}_{AB}$, the index AB specifies the direction

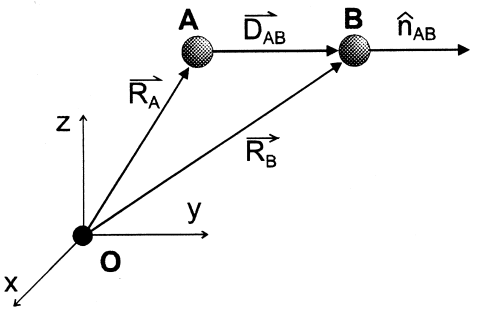

* Corresponding author.

0166-1280/99/$ - see front matter
PII: S0166-1280(98)00498-9

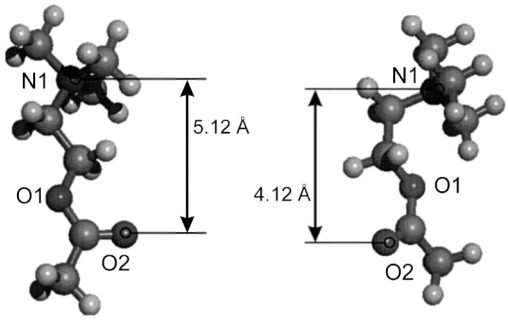

Fig. 1. Two conformers of acetylcholine Left: *anti–anti* conformer involving the N_1–C–C–O_2 and the C–C–O_2–CO torsional modes. Optimized Ni…O_1 distance = 5.12 Å (biological prediction for maximum separation = 5.9 Å). Right: *gauche–gauche* conformer involving the N_1–C–C–O_2 and the C–C–O_2–CO torsional modes. Optimized Ni…O_1 distance = 4.12 Å (biological prediction for maximum separation = 4.4 Å).

All vectors have *x*, *y*, and *z* components with respect to a right handed Cartesian coordinate system.

2. Introduction

The ability of the modern chemist and biologist to design, synthesize, and modulate peptide structures, for fundamental or applied research, will depend on the understanding of the conformational and topological properties of peptides in relation to their biological activities.

Multiple conformations provide a mechanism for biological survival since conformational selectivity leads to biological selectivity. Nature can utilize different conformational properties in response to changes that occur at receptors or other structures of biological significance with which a peptide interacts. A classical example is acetylcholine, where the two possible conformations, the gauche and anti, can dock, and, therefore, complex with two different receptors, the muscarinic and nicotinic receptors, respectively [1], as illustrated in Fig. 1.

Even a modest number of rotating bonds, in a moderately sized compound, lead to a very large number of conformers. It is necessary, therefore, to make a systematic search of all conformational possibilities, from which the selection of a limited number of plausible starting conformations may be chosen. Low-energy structures can be generated from such a subset, by means of appropriate energy minimization procedures. The torsional angles and therefore the interatomic distances of a molecule cannot simultaneously assume arbitrary values. Only discrete conformations may exist, representing a particular combination of values of torsional angles, whose explicit description is essential to the problems of molecular conformation [2]. Fig. 2 illustrates the torsional angles involved in the folding of a general peptide or protein segment. The Fig. suggests that the choice of conformations is continuous about the cones

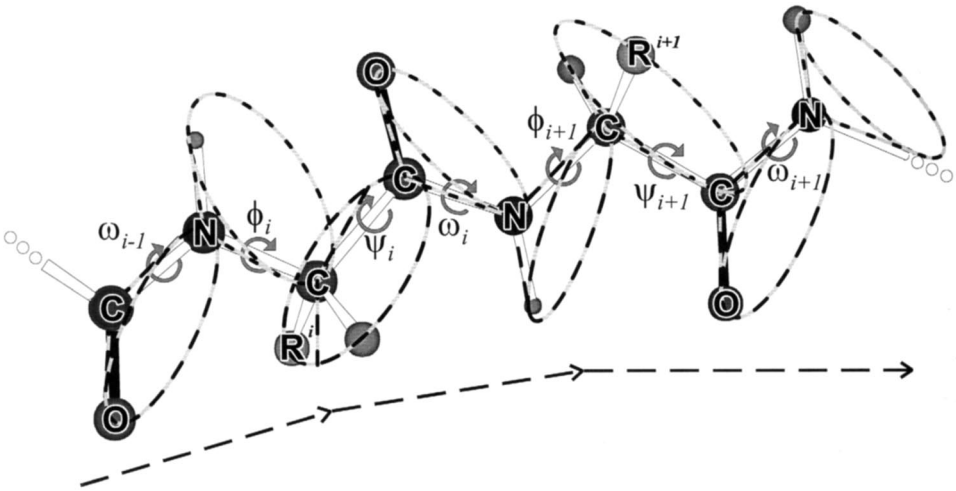

Fig. 2. A schematic illustration of the conformational modes of motion in a general protein segment involving the *i*th and $(i + 1)$st amino acids. The conical spatial requirement for each torsional modes are clearly shown.

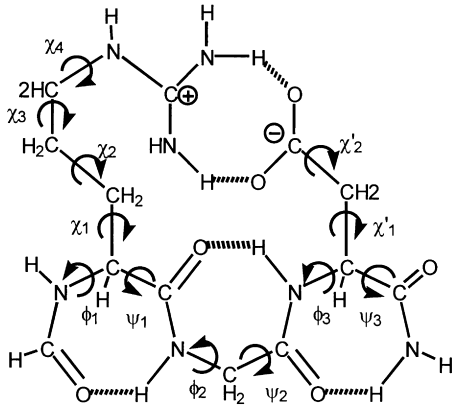

Fig. 3. A schematic illustration of a particular conformation of *N*-formyl RGD amide shown as HCO-HN-R-G-D-CONH (i.e. HCO-HN-Asp-Gly-Arg-CONH). The backbone conformation is shown as γ_2 (i.e. $\theta_i \approx -60°$; $\psi_1 \approx +60°$for $1 \leq i \leq 3$). The side-chain conformation is depicted as such that the guanidinium ion and the carboxylate ion could form a ''salt bridge''.

of each of these torsions. Yet, in reality, the process is 'quantized' since only discrete conformers are stable and only these structures correspond to physical reality. Along ϕ and ψ only *gauche* (+) or g^+ (+60°), *anti* or *a* (+ or −180°) and *gauche* (−) or g^- (−60° or +300°) are stable conformers. Along ω only the *syn* or *cis* peptide bond (0°) and the *anti* or *trans* peptide bond (+ or −180°) represent stable structures. Modern computer, hardware and software have made it possible to examine the conformational properties of small peptides by ab initio quantum mechanical calculations [3–34]. However, it is clear that for compounds containing a great number of torsional angles, the conformational search using a 'brute-force' procedure is too time consuming.

We present here a geometrical approach, based on very simple mathematical principles, with the principal goal being the evaluation, in a fast and an inexpensive way, of all the conformational possibilities of a flexible molecule. Once the corresponding overall conformational behavior of the molecule has been obtained, we could choose conformations which might be calculated using either a simple or a sophisticated energy minimization procedure. Since interatomic distances are related to the energy and other experimentally observable parameters of the conformation (e.g. NMR) in a relatively direct and canonical way, the potential advantages of this approach are apparent.

Our objective in this paper is two-fold. First, we wish to map out the space that can be spanned by a moiety of a flexible molecule. This may be important in studying the spatial requirement of a side-chain of an amino acid residue in a peptide or in a protein. This is important for our understanding of side-chain–side-chain interaction as may be the case for the Arg-Gly-Asp (RGD) [35–37] motif (Fig. 3). Second, we wish to automate input file generations for force field or semi-empirical or ab initio molecular computations. This amounts to nothing less than creating a software in which the basic principles of multidimensional conformational analysis (MCDA) are coded. Again we may use RGD as an example (Fig. 3).

Assuming that only *trans* peptide bond are considered we may recognize six torsional angles (ϕ_1, ψ_1, ϕ_2, ψ_2, ϕ_3, ψ_3) associated with the RGD backbone. These lead to $3^6 = 729$ backbone conformers. We may recognize six torsional angles (χ_1, χ_2, χ_3, χ_4 as well as χ_1' and χ_2') associated with the side-chain of arginine and aspartic acid. These lead to $3^6 = 729$ side-chain conformers for each backbone structures. The total number of conformers, therefore, is expected to be

$$N_0 = 3^6 \times 3^6 = 729 \times 729 = 531441$$

Clearly, a pre-search as well as the automation of input file generation will be necessary to study such problems in their completeness.

The present report itself consist of two parts. The first part is primarily devoted to the mathematical formulation of our approach. The second part of the paper reports possible applications to saturated fluorohydrocarbons.

3. Mathematical formalism

We consider several successive rotations (Scheme 1):

along the directions of $\overrightarrow{AB}$
along the directions of $\overrightarrow{BC}$ and
along the directions of $\overrightarrow{CD}$

Every atom, is characterized by its Cartesian coordinates, and therefore these coordinates are the position

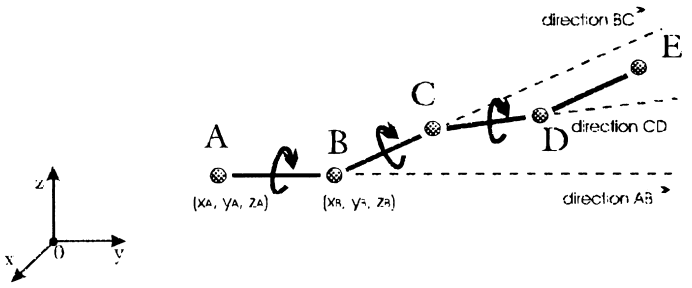

Scheme 1.

vectors pointing from origin O to that atom:

$$atomA \rightarrow \vec{R}_A \equiv (x_A, y_A, z_A) \tag{1}$$

$$atomB \rightarrow \vec{R}_B \equiv (x_B, y_B, z_B) \ldots, \ etc.$$

We may suppose, that all atoms connected directly or indirectly to atom B (such as C, D, etc.), rotate about the AB axis (i.e. about direction $\overrightarrow{AB}$) as shown in the following diagram (Scheme 2):

Thus, in this first rotation all the connected atoms C, D, E, etc. will rotate about the AB axis. The points O_C, O_D, O_E, etc. are the centers of the rotations for atoms C, D, E, etc. with radii r_C, r_D, r_E, etc., respectively (Scheme 2).

In the second rotation about the BC axis (i.e. direction $\overrightarrow{BC}$), the coordinates of the atoms B and C do not vary. The atoms A, B and C, are maintained fixed throughout this process. (Scheme 3). However, for every rotamer generated by the first rotation (about the $\overrightarrow{AB}$ axis) a full second rotation (about the $\overrightarrow{BC}$ axis) is possible.

In the second rotation, the point O‘$_D$ is the new center of rotation of atom D, in the direction of $\overrightarrow{BC}$ with radius r‘$_D$ (Scheme 3).

Further rotations (the 3rd one is along $\overrightarrow{CD}$) will follow the same procedure. The mathematical relationships necessary, can easily be derived from the first and second rotations discussed earlier.

1. To define the centers of rotations (e.g. O_C), the following equations need to be considered.

   (a) The vector along the $\overrightarrow{AB}$ direction is denoted as $\vec{D}_{AB}$ and it may be generated as a vectorial difference:

$$\vec{D}_{AB} = \vec{R}_B - \vec{R}_A \tag{2}$$

   as shown in Scheme 4. Similarly, we may define the vector along the $\overrightarrow{BC}$ direction:

$$\vec{D}_{BC} = \vec{R}_C - \vec{R}_B \tag{3}$$

   (b) The unit vector $\hat{n}_{AB}$, pointing along the direction $\overrightarrow{AB}$, is:

$$\hat{n}_{AB} = \frac{\vec{D}_{AB}}{|\vec{D}_{AB}|} = \frac{\vec{R}_B - \vec{R}_A}{|\vec{R}_B - \vec{R}_A|} \tag{4}$$

   The *x*, *y* and *z* component of $\hat{n}_{AB}$ are given later in

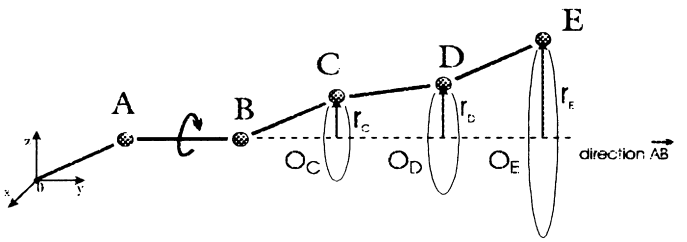

Scheme 2.

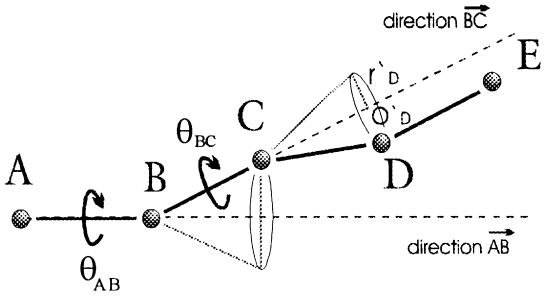

Scheme 3.

equation (5):

$$(\hat{n}_{AB})_x = \frac{x_B - x_A}{\sqrt{\left((x_B - x_A)^2 + (y_B - y_A)^2 + (z_B - z_A)^2\right)}}$$

$$(\hat{n}_{AB})_y = \frac{y_B - y_A}{\sqrt{\left((x_B - x_A)^2 + (y_B - y_A)^2 + (z_B - z_A)^2\right)}} \quad (5)$$

$$(\hat{n}_{AB})_z = \frac{z_B - z_A}{\sqrt{\left((x_B - x_A)^2 + (y_B - y_A)^2 + (z_B - z_A)^2\right)}}$$

(c) In agreement with Scheme 4 the distance of O_C measured from atom B, may be defined as:

$$d_{B-O_C} = \left|\vec{D}_{BC}\right| \cdot \cos\alpha \quad (6)$$

If we multiply the right hand side of this equation with $|\hat{n}_{AB}|$, which is unity, then we obtain the expression of the dot product of the two vectors involved $\hat{n}_{AB}$ and $\vec{D}_{BC}$:

$$d_{B-O_C} = |\hat{n}_{AB}|\left|\vec{D}_{BC}\right| \cdot \cos\alpha$$

This being the case d_{B-O_C} may also be generated from the components of $\hat{n}_{AB}$ and $\vec{D}_{BC}$ as the following dot product of the two vectors.

$$(\text{distance})_{B-O_C} \equiv d_{B-O_C} = \hat{n}_{AB} \bullet \vec{D}_{BC}$$

$$= \left[(n_{AB})_x (n_{AB})_y (n_{AB})_z\right] \begin{bmatrix} (x_C - x_B) \\ (y_C - y_B) \\ (z_C - z_B) \end{bmatrix} \quad (7)$$

Thus

$$d_{B-O_C} = (\vec{n}_{AB})_x (x_C - x_B) + (\vec{n}_{AB})_y (y_C - y_B) + (\vec{n}_{AB})_z (z_C - z_B) \quad (8)$$

(d) The position vector for O_C ($\vec{R}_{O_C}$) with respect to the origin O is:

$$\vec{R}_{O_C} = \vec{R}_B + d_{B-O_C}\hat{n}_{AB} \quad (9)$$

For all the atoms, the procedure is similar to the first rotation about AB. For example, the position vector for O_D, associated with atom D, may be written the following way:

$$\vec{R}_{O_D} = \vec{R}_B + d_{B-O_D}\hat{n}_{AB} \quad (10)$$

where

$$d_{B-O_D} = \hat{n}_{AB} \cdot \vec{D}_{BD} \quad (11)$$

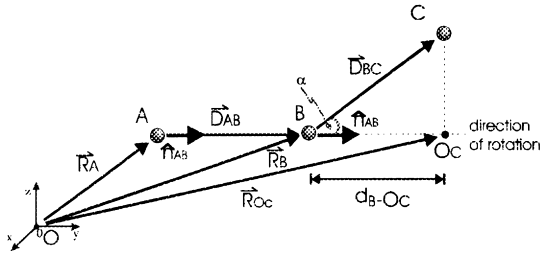

Scheme 4.

2. In order to generate the coordinates of the points as a function of the rotational angle increment $\Delta\theta$, we consider the following relationships:

(a) The definition of an auxiliary vector

$$\vec{\theta} = (\Delta\theta)\hat{n}_{AB} \quad (12)$$

where $\Delta\theta$ is a constant increment in the angle of rotation (Scheme 5)
If $\Delta\theta = 5°$ then a full rotation corresponds to $72 \times 5° = 360°$. Consequently, for a rotation of an

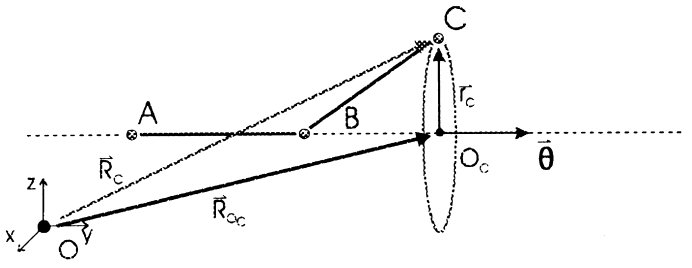

Scheme 5.

angle θ_{AB} about the direction $\overrightarrow{AB}$ we may write

$$\theta_{AB} = k(\Delta\theta) \tag{13}$$

Note that the length of $\vec{\theta}$ is: $|\vec{\theta}| = \Delta\theta =$ *the increment in* θ

(b) The definition of the vector $\vec{r}_C$ is

$$\vec{r}_C = \vec{R}_C - \vec{R}_{O_C} \tag{14}$$

with the following components: (Scheme 5)

$$(\vec{r}_C)_x = \left(x_C - x_{O_C}\right)$$

$$(\vec{r}_C)_y = \left(y_C - y_{O_C}\right) \tag{15}$$

$$(\vec{r}_C)_z = \left(z_C - z_{O_C}\right)$$

where

$$\vec{R}_{O_C} = \left(x_{O_C}, y_{O_C}, z_{O_C}\right) \tag{16}$$

The definition of the following cross product:

$$\vec{\Delta}r = \vec{r}_C \times \vec{\theta} = \Delta\theta(\vec{r}_C \times \hat{n}_{AB}) \tag{17}$$

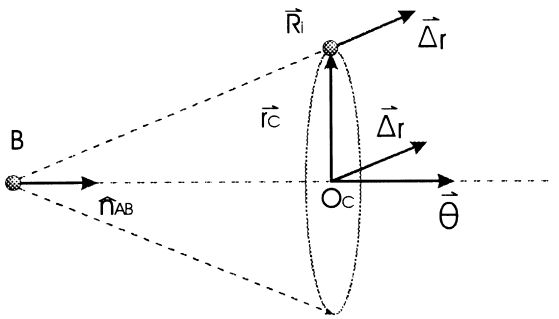

Scheme 6.

is shown in (Scheme 6) where the length of $\vec{\Delta}r$, is defined as follows:

$$\left|\vec{\Delta}r\right| = |\vec{r}_C|\Delta\theta \equiv r_C\Delta\theta \tag{18}$$

To produce a new point, the use of the above definition of $\vec{\Delta}r$ is rigorously correct for an infinitesimal angle change $\Delta\theta$. However, for a finite angle of $\Delta\theta$, it is necessary to make a corrections.

(d) For the corrections, we need to consider the following: for a rotation of angle $\Delta\theta$, we need to know $\vec{\Delta}r'$ (Scheme 7). Note the relationship given in Eq. (19)

$$\sin(\Delta\theta/2) = \frac{\frac{1}{2}|\vec{\Delta}r'|}{|\vec{r}_C|} \tag{19}$$

and, therefore, the length of $\vec{\Delta}r'$ becomes related

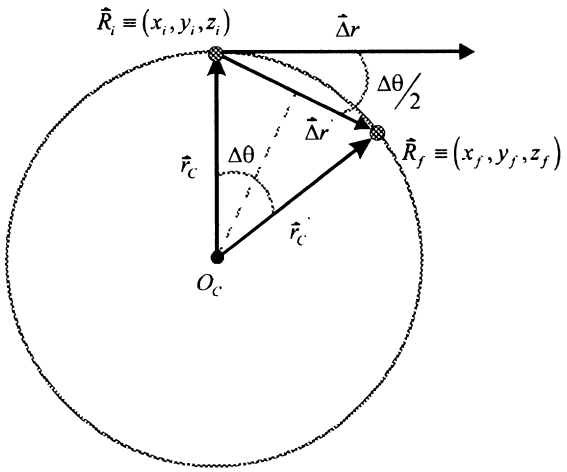

Scheme 7.

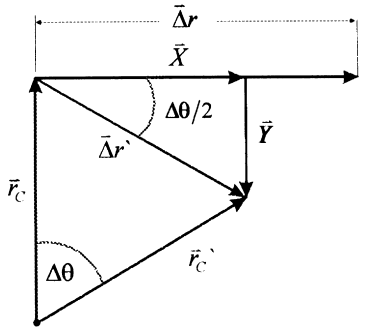

Scheme 8.

to the change in rotational angle $\Delta\theta$:

$$\left|\vec{\Delta}r'\right| = 2|\vec{r}_C|\sin(\Delta\theta/2) \tag{20}$$

If we know $\vec{R}_i$, which could be the initial position vector for point C, (i.e. $\vec{R}_C$) then the final position vector ($\vec{R}_f$) or the new point after rotation by $\Delta\theta$, may be defined as:

$$\vec{R}_f = \vec{R}_i + \vec{\Delta}r' \tag{21}$$

(e) We need to define two unit vectors, along the directions of the vectors $\vec{\Delta}r$ and $\vec{r}_C$ which are perpendicular to each other.

$$\hat{\Delta}r = \frac{\vec{\Delta}r}{|\vec{\Delta}r|} \tag{22}$$

$$\hat{r}_C = \frac{\vec{r}_C}{|\vec{r}_C|} \tag{23}$$

(f) The vector $\vec{\Delta}r'$, may be defined as the sum of the two orthogonal vectors $\vec{X}$ *and* $\vec{Y}$ (Scheme 8)

$$\Delta r' = \vec{X} + \vec{Y} \tag{24}$$

where

$$\vec{X} = \left|\vec{X}\right|\hat{\Delta}r \tag{25}$$

$$\vec{Y} = \left|\vec{Y}\right|(-\hat{r}_C) \tag{26}$$

The lengths of the $\vec{X}$ and $\vec{Y}$ vectors are obtained through the following relationships:

$$\left|\vec{X}\right| = \left|\vec{\Delta}r'\right|\cos(\Delta\theta/2) = 2|\vec{r}_C|\sin(\Delta\theta/2)\cos(\Delta\theta/2) \tag{27a}$$

or

$$\left|\vec{X}\right| = |\vec{r}_C|\sin(\Delta\theta) \tag{27b}$$

Thus, using Eqs. (18) and (22) we obtain Eq. (28)

$$\vec{X} = \left|\vec{X}\right|\hat{\Delta}r = \left(\frac{\sin(\Delta\theta)}{\Delta\theta}\right)\vec{\Delta}r \tag{28}$$

Similarly:

$$\left|\vec{Y}\right| = \left|\vec{\Delta}r'\right|\sin(\Delta\theta/2) = 2|\vec{r}_C|\sin^2(\Delta\theta/2)$$

or

$$\left|\vec{Y}\right| = |\vec{r}_C|[1 - \cos(\Delta\theta)] \tag{29}$$

resulting in the following relationships

$$\vec{Y} = \left|\vec{Y}\right|(-\hat{r}) = [1 - \cos(\Delta\theta)](-\vec{r}_C) \tag{30}$$

(g) Since

$$\vec{\Delta}r' = \vec{X} + \vec{Y} \tag{31}$$

therefore the vector $\vec{\Delta}r'$ is:

$$\vec{\Delta}r' = \left(\frac{\sin\Delta\theta}{\Delta\theta}\right)\vec{\Delta}r + [1 - \cos(\Delta\theta)](-\vec{r}_C) \tag{32}$$

Noting that Eq. (17)

$$\vec{\Delta}r = \vec{r}_C \times \vec{\theta} = \Delta\theta(\vec{r}_C \times \hat{n}_{AB})$$

We may substitute this equivalence into Eq. (32) and obtain Eqs. (33)

$$\vec{\Delta}r' = \left[\frac{\sin(\Delta\theta)}{\Delta\theta}\right]\Delta\theta(\vec{r}_C \times \hat{n}_{AB}) + [1 - \cos(\Delta\theta)] \times (-\vec{r}_C) \tag{33a}$$

We can now express $\vec{\Delta}r'$ as follows:

$$\vec{\Delta}r' = [\sin(\Delta\theta)](\vec{r}_C \times \hat{n}_{AB}) + [1 - \cos(\Delta\theta)](-\vec{r}_C) \tag{33b}$$

(h) The final or new position vector after rotation

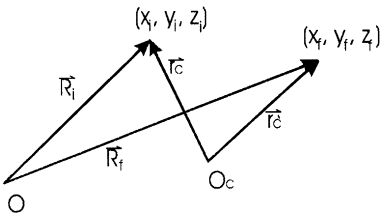

Scheme 9.

by $\Delta\theta$, is:

$$\vec{R}_f = \vec{R}_i + [\sin(\Delta\theta)](\vec{r}_C \times \hat{n}_{AB}) + (1 - \cos\theta)(-\vec{r}_C) \quad (34)$$

(i) The Cartesian vector components for this final position vector, are:

$$x_f = x_i + \sin\Delta\theta(\vec{r}_C \times \hat{n}_{AB})_x - (1 - \cos\Delta\theta) \times \left(x_i - x_{O_C}\right) \quad (35)$$

$$y_f = y_i + \sin\Delta\theta(\vec{r}_C \times \hat{n}_{AB})_y - (1 - \cos\Delta\theta) \times \left(y_i - y_{O_C}\right)$$

$$z_f = z_i + \sin\Delta\theta(\vec{r}_C \times \hat{n}_{AB})_z - (1 - \cos\Delta\theta) \times \left(z_i - z_{O_C}\right)$$

where the components for the cross product $\vec{\Delta}r' = \vec{r}_C \times \hat{n}_{AB}$, may be written in detail, as follows:

$$(\vec{r}_C \times \hat{n}_{AB})_X = \left(y_i - y_{O_C}\right)(\hat{n}_{AB})_Z - \left(z_i - z_{O_C}\right)(\hat{n}_{AB})_Y \quad (36)$$

$$(\vec{r}_C \times \hat{n}_{AB})_Y = \left(z_i - z_{O_C}\right)(\hat{n}_{AB})_X - \left(x_i - x_{O_C}\right)(\hat{n}_{AB})_Z$$

$$(\vec{r}_C \times \hat{n}_{AB})_Z = \left(x_i - x_{O_C}\right)(\hat{n}_{AB})_Y - \left(y_i - y_{O_C}\right)(\hat{n}_{AB})_X$$

(j) In order to continue the overall process, the vector $\vec{r}_C$ has been changed to $\vec{r}_C{}'$ (Scheme 8) after the rotation by $\Delta\theta$. Note that

$$|\vec{r}'_C| = |\vec{r}_C| \quad (37)$$

With the knowledge of $\vec{R}_f$, the vector $\vec{r}_C{}'$ may be calculated (Scheme 9):

$$\vec{r}'_C = \vec{R}_f - \vec{R}_{O_C} \quad (38)$$

As the result of all of these, the new cross product $\vec{r}_C{}' \times \hat{n}_{AB}$ may be computed.

(k) We calculate the new position after rotation by $\Delta\theta$ and successively we continue until one full revolution is completed.

4. Computational methods

4.1. Input data

It should be emphasized that for the previous procedure to work, it is necessary to know the initial atomic coordinates that change during the rotation. This implies that bond lengths and bond angles must be given in order to calculate the Cartesian coordinates of the atoms. In the present exploratory study all the bond angles were taken to the tetrahedral (109° 28′) and the following average bond lengths were used:

C–H = 1.089Å
C–C = 1.540Å
C–F = 1.330Å

Standard bond length may be taken from classical books [38] or from any more recent computational database [39].

4.1.1. GASCOS Program

Written for PC using Mathlab (Mathsoft Inc.) program and running under MS Windows operating system. The program was thoroughly tested before it was applied to molecular system.

4.1.2. Ab initio Geometry optimization

Gaussian 94 [40] was used for the control calculations at the HF/6-31G level of theory.

5. Applications

Basically, we can consider two types of application of the previous method which are independent of the nature of the conformationally flexible molecule to be

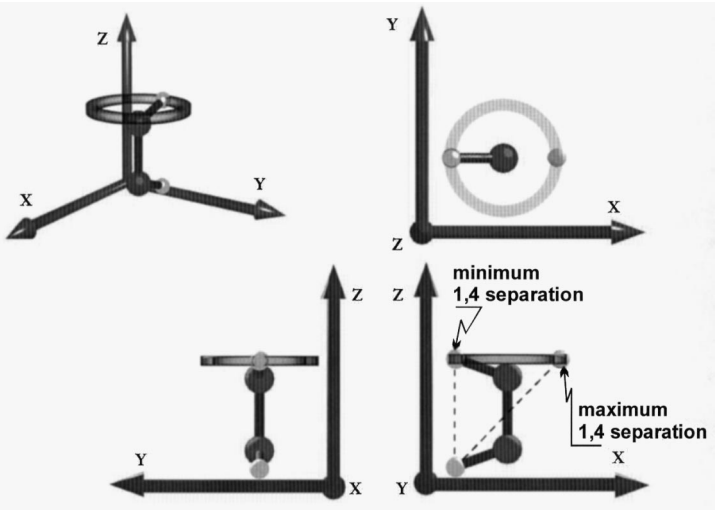

Fig. 4. Top, front, side and perspective views of the circular motion in ethane involving θ_{AB}.

studied. These two types of application provide answers to the following two questions:

(i) How close can two non-bonded moieties approach each other within a given molecule during conformational change?
(ii) Could one automate the generation of input data, for a geometry optimization of a molecule that has many internal rotations (i.e. it is multiple rotor) using the rules of multidimensional conformational analysis (MCDA)?

The first of these applications could require a relatively small increment in rotation ($\Delta\theta$ could be 5° or perhaps 10°) while the second one may involve a relatively large increment in rotation ($\Delta\theta$ may be 120°).

5.1. Mapping steric proximity or spatial availability for substituents during conformational change

Ethane is one of the simplest examples as it has only one torsional angle.

The motion of one of the hydrogen atoms (within the rotating methyl group) with respect to the other hydrogen atoms (within the non-rotating methyl group) is shown in Fig. 4. Clearly the motion is circular as it is shown as top, front and side views. A general perspective is also included in Fig. 4. The circular motion is also clear in Fig. 5 which is shown by the 72 small circles (corresponding to $\Delta\theta = 5$) on the top of the cube. This Fig. also shows the various non-vectorial (e.g. $d_{B\text{-}O_C}$) and vectorial (R_A, R_B, R_C, etc.) quantities used in the mathematical derivation of the method.

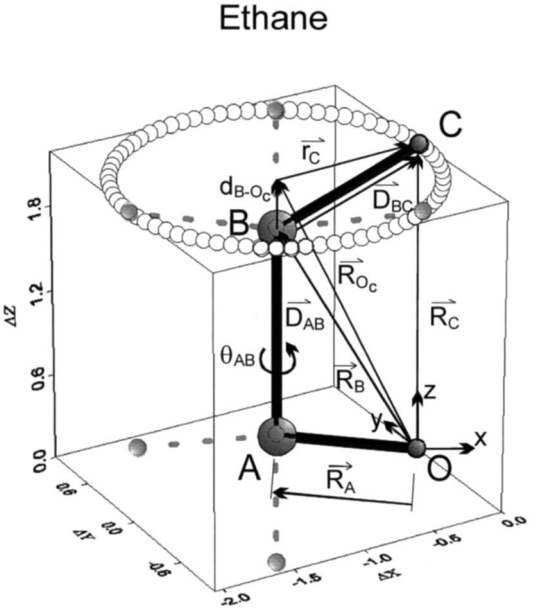

Fig. 5. Separation of the two terminal hydrogens (a 1,4 separation) in the eclipsed ethane. The lower two shaded circles show the H atoms attached to carbon A and upper three shaded circles show the position of the three H atoms attached to carbon B when ethane is its staggered conformation.

The separation of the two terminal hydrogen atoms is denoted by the vector $\vec{R}_C$ in Fig. 5. The absolute value of $\vec{R}_C$ can be expressed in terms of the torsional angle θ_{AB}

$$\left|\vec{R}_C\right| = f(\theta_{AB}) \tag{40a}$$

$$\left|\vec{R}_C\right| = \sqrt{\left(|R_C^i|^2 + 2\left|\vec{r}_C^{(i)}\right|^2(1-\cos\theta_{AB}) + 2\vec{R}_C^{(i)}\cdot(\hat{n}_{AB}\times\vec{r}_C)^{(i)}\sin\theta_{AB} + 2\vec{R}_C^{(i)}\cdot\vec{r}_C^{(i)}(\cos\theta_{AB}-1)\right)} \tag{40b}$$

Note that the superscript i indicates the various values which were initially evaluated when θ_{AB} is equal to zero.

For the particular case of ethane and observing Fig. 5 it is possible to consider that $\vec{R}_C^{(i)}$ is perpendicular to the cross product $(\hat{n}_{AB}\times\vec{r}_C)^{(i)}$ and therefore

$$2\vec{R}_C^{(i)}\cdot(\hat{n}_{AB}\times\vec{r}_C)^{(i)} = 0 \tag{41}$$

Consequently only the terms involving the function

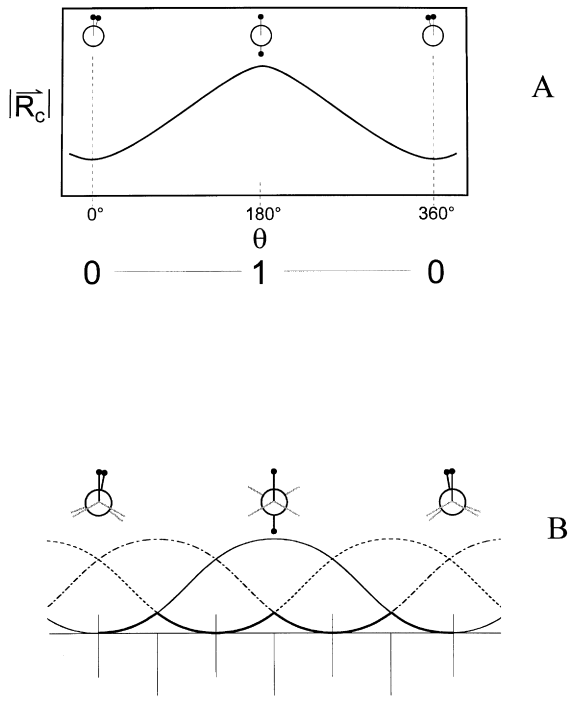

Fig. 6. Functional variation of the 1,4 separation of the two terminal hydrogen atoms (denoted by $|\vec{R}_C|$) with the torsional angle θ_{AB} [c.f. Eq. (40)].

$\cos\theta_{AB}$ will not vanish.

$$\left|\vec{R}_C\right| = \sqrt{5.11 + 2.07(1-\cos\theta_{AB})} \tag{40c}$$

The final form, Eq. (40c) was obtained by using the bond lengths and bond angles specified under the heading 'Input Data' in the Computational Methods section.

The variation of this function with θ_{AB} is shown in Fig. 6. Extrema calculation

$$\frac{d\left|\vec{R}_C\right|}{d\theta_{AB}} = 0$$

yields $\theta_{AB} = 0°$ or 360° for the minimum separation and $\theta_{AB} = 180°$ for the maximum separation.

Note, that the function is periodic and that its minimum and maximum may be characterized by the number of negative second derivatives as the index (λ) of these critical points. This is shown as a strings of numbers (0–1–0) on the bottom of Fig. 6A. Fig. 6A shows the distance between H^0 and H^C. However, as H^C is rotated away from H^0, the other H atom of the rotating methyl group come to replace H^C. Thus, we may have three curves, like the one shown in Fig. 6A shifted by $+120°$ and $-120°$ away from the original curve. These three curves are shown in Fig. 6B. The minimum separation between H^0 and any one of the three H atoms of the rotating CH_3 group is shown by the bold curve. This bold curve looks like an opposite of a potential energy curve like the one shown later at the top of Fig. 19.

Propane is a double rotor; therefore we have two different torsional angles: θ_{AB} and θ_{BC}.

Consequently, there are two different circular motions. The top, front and side views as well as

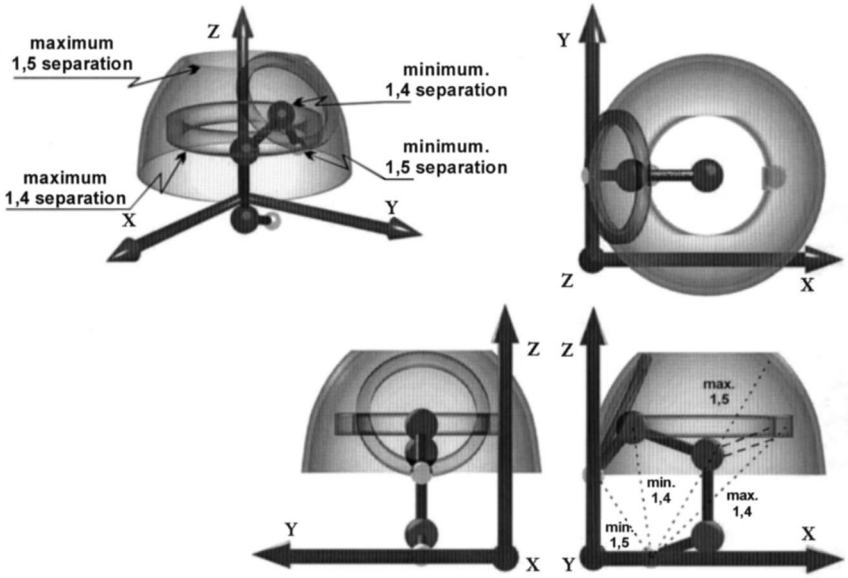

Fig. 7. Top, front, side and perspective views of the circular motion in propane involving both θ_{AB} and θ_{BC}.

general perspective of these circular motions, are shown in Fig. 7. The distance between the first hydrogen and the last carbon (H–C–C–C) is a 1,4 separation. It is like the H–C–C–H separation in ethane (Fig. 5); it depends on only one torsional angle (θ_{AB}). However, the distance between the first and last hydrogen atoms (H–C–C–C–H) is a 1,5 separation. The calculation of this separation is a bit more complex because it includes the variation of two torsional angles (θ_{AB} and θ_{BC}).

Thus while ethane (Fig. 4) had only one circle, propane (Fig. 7) had the combination of the two circular motions leading to a dome like 'lamp-shade' object.

Fig. 8 shows the motion of the terminal hydrogen again using $\Delta\theta = 5°$ increment. The top circle has the points where the H–C–C–C–H 1,5 separation is at its maximum, while the bottom circle has the points where the 1,5 separation is at its minimum. The minimum and maximum 1,4 separation (i.e. H–C–C–C) are located at about half way up of the 'lamp shade' object.

The 1,4 separation $|\vec{R}_C|$ of propane is similar in form to Eq. (40c), but the constants are different as the C–C bond length is longer than the C–H bond length:

$$\left|\vec{R}_C\right| = \sqrt{[6.01 + 296(1 - \cos\theta_{AB})]} \tag{42a}$$

$$\left|\vec{R}_D\right| = f(\theta_{AB}, \theta_{BC}) \tag{42b}$$

Using a more general separation function, Eq. (42b), we can locate 1,5 minimum and maximum separations. This is shown in Fig. 9. This Fig. is generated numerically since it was not trivial to obtain function Eq. (42b) in analytic form.

$$\left[\left(\frac{\partial\left|\vec{R}_D\right|}{\partial\theta_{AB}}\right), \left(\frac{\partial\left|\vec{R}_D\right|}{\partial\theta_{BC}}\right)\right] = [0, 0] \tag{43}$$

The extrema calculations were also a bit more complicated than before. Since partial derivatives were required here. The gradient vector needed to vanish for the minimum and maximum distances of the 1,5 separation. Fig. 9 shows $|\vec{R}_D|$, according to Eq. (42b), and the location of the extrema are clearly seen. There is one unique maximum ($\lambda = 2$) which occurs once (at the center) and one unique minimum ($\lambda = 0$) which occurs four times at the four equivalent corners. The distance surface also has two equivalent critical points

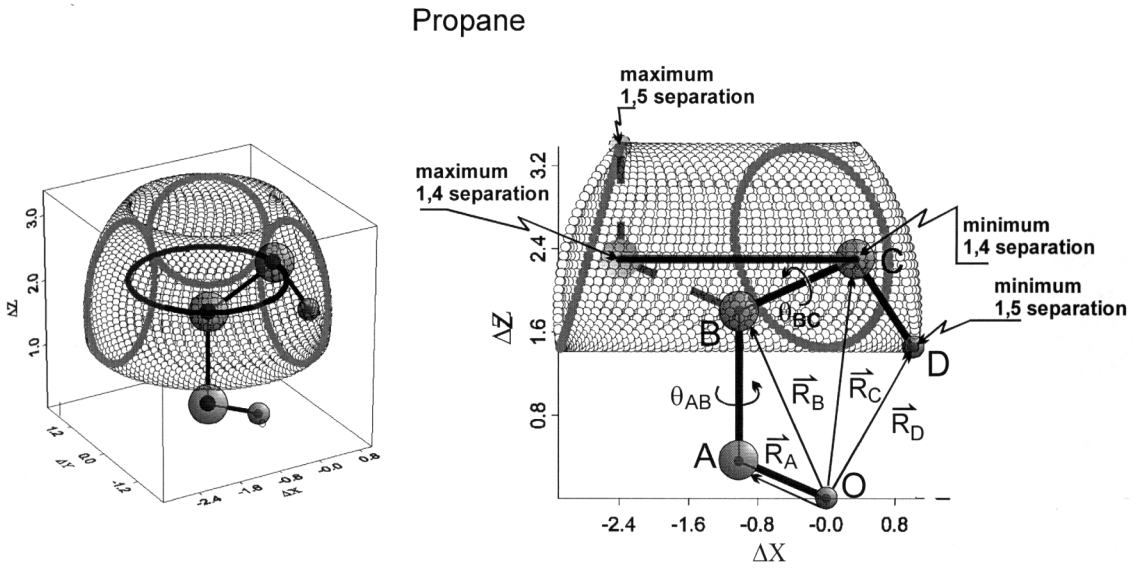

Fig. 8. Separation of the two terminal hydrogens (a 1,5 separation) in propane. The 1,4 (H^{O}–C^{C}) separation is also shown for comparison.

of index 1 (i.e. $\lambda = 1$) located on the four edges. Two opposing edges have identical pairs of saddle points ($\lambda = 1$).The schematic topology of function (42b), given in Fig. 9, is shown in Fig. 10. At the bottom and left hand side edges, the topology (0–1–0) of the single rotations, corresponding to the 1,4 separations, are also given. Note that the functional shape of the single rotation is shown in Fig. 6A.

Here again, just like in Fig. 6B there is a three-fold repetition with both methyl groups. Thus, the single maximum shown at the centre of Fig. 9 is separated three times along θ_{AB} and three times along θ_{BC} The result is $3 \times 3 = 9$ maxima on the distance surface. Again, such a distance surface, which is a function of the torsional angles, look like the opposite of the potential energy surface (PES) like the one shown later in Fig. 20.

In propane we may recognize the following distinctly different separations

$$\begin{aligned} &1,4\ \textit{separation} \quad H^{O}\ldots C^{C} \quad \textit{same as}\ C^{A}\ldots H^{D} \\ &1,5\ \textit{separation} \quad H^{O}\ldots H^{D} \end{aligned} \tag{44}$$

The 1,4 separation is analogous to the $H^{O}\ldots H^{C}$ separation in ethane (c.f. Scheme 10). Consequently, the propane case may be regarded, at least topologically, as a monosubstituted ethane (45a)

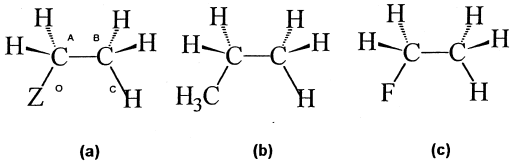

(45)

Of course if Z = CH_3 (45b) then only the carbon atom of the substituting CH_3 group is considered and the hydrogens of the substituting CH_3 group are ignored. If Z = F (45c) then, apart from the difference in C–H and C–F bond length, the situation will be equivalent to ethane.

Butane is a triple rotor and, therefore, its conformational change is governed by three circular motions involving θ_{AB}, θ_{BC} and θ_{CD} (Scheme 12).

In this case not a single dome but a ‘hyperdome’ consisting of an infinite number of domes describe the spatial requirements of the rotating groups. Four of such domes, rotated 90 apart of each other, are shown in Fig. 11.

In butane we may recognize, in accordance with Scheme 12, the following distinctly different

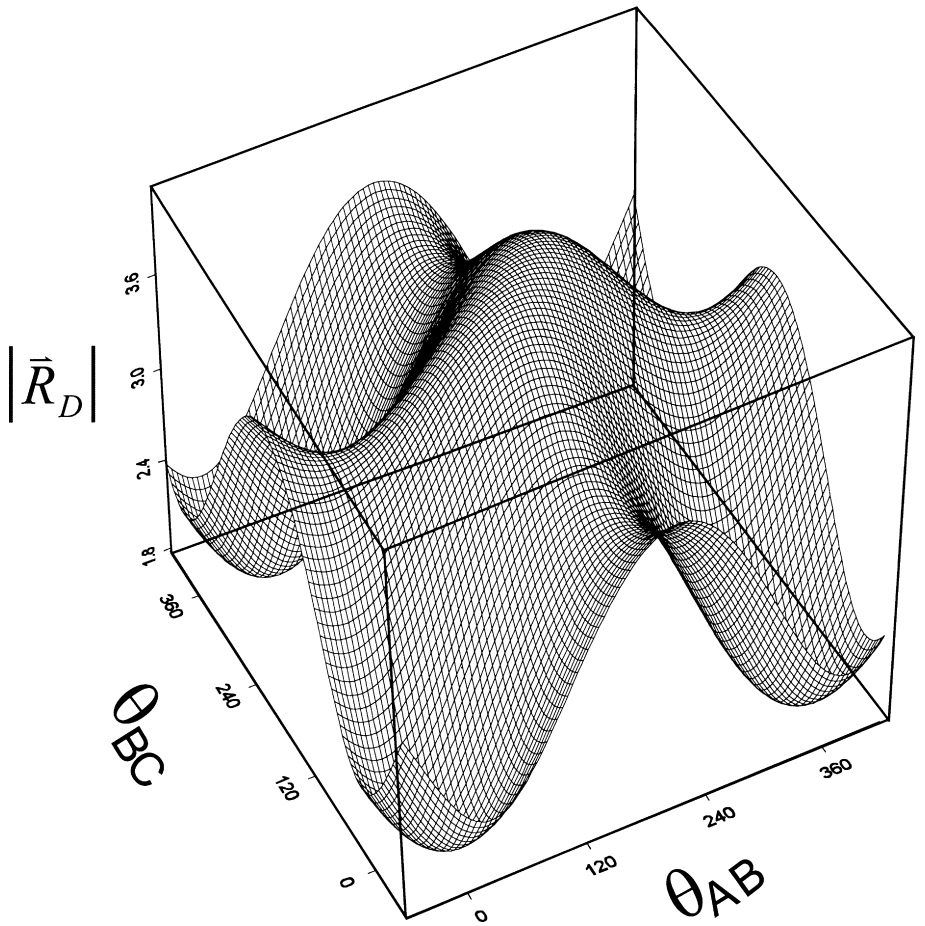

Fig. 9. Functional variation of the 1,5 separation of the two terminal hydrogen atoms (denoted by $|\vec{R}_C|$) in propane with the torsional angles θ_{AB} and θ_{BC} [c.f. Eq. (42)].

separations:

$$
\begin{aligned}
&1,4\ \textit{separation} \quad \begin{cases} H^O \ldots C^C \\ C^A \ldots C^D \end{cases} \quad (\textit{same as } C^B \ldots H^E) \\
&1,5\ \textit{separation} \quad H^O \ldots C^D \quad (\textit{same as } C^A \ldots H^E) \\
&1,6\ \textit{separation} \quad H^O \ldots H^E
\end{aligned} \tag{46}
$$

Fig. 12 shows the motion of the two non-equivalent 1,4 separations together with a 1,5 and 1,6 separations.

The 1,4 separation is analogous to the $H^O \ldots H^C$ separation in ethane and the $H^O \ldots C^C$ (or its equivalent $C^A \ldots H^D$) separation in propane. Also the 1,5 separation is analogous to the $H^O \ldots H^D$ separation in propane. Consequently, the butane case may be regarded, at least topologically, as the 1,2-disubstituted ethane of the 1-monosubstituted propane Eq. (47).

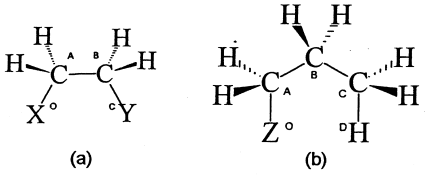

(47)

On the basis of Fig. 10 it is easy to predict where the minimum and maximum separations are located.

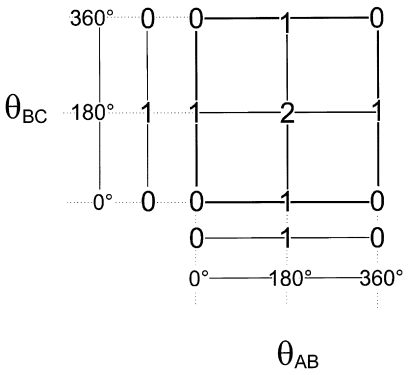

Fig. 10. Topology of the $|\vec{R}_D| = f(\theta_{AB}, \theta_{BC})$ separation function [c.f. Eq. (42)]. Critical point are denoted by their index: minimum is 0, saddle point is 1 and maximum is 2. The topologies of single rotations are denoted as 0–1–0 and are shown as a horizontal and vertical lines at the bottom for θ_{AB} and the left band side for θ_{BC}, respectively.

$$\text{minimum separation}: \quad \theta_{AB} = \theta_{BC} = \theta_{CD} = 0^\circ \tag{48}$$

$$\text{maximum separation}: \quad \theta_{AB} = \theta_{BC} = \theta_{CD} = 180^\circ$$

These are denoted as 0 (i.e. $\lambda = 0$) and 3 (i.e. $\lambda = 3$) on the topological presentation of the distance hypersurface

$$\left|\vec{R}_E\right| = f(\theta_{AB}, \theta_{BC}, \theta_{CD}) \tag{49}$$

as shown in Fig. 13.

Pentane is a quadruple rotor and therefore its conformational change is governed by four circular motions involving θ_{AB}, θ_{BC}, θ_{CD} and θ_{DE}.

In the case of three torsional angles the motions were characterized by a 'hyperdome'(Fig. 11) which could not be drawn fully. In the case of pentane, because of the added fourth torsional angle the 'super-Hyperdome' cannot be graphically presented even in a schematic way. However, we may recognize two 1,4, two 1,5, one 1,6 and one 1,7 interactions, in accordance with Scheme 13. These are summarized in

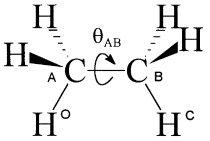

Scheme 10.

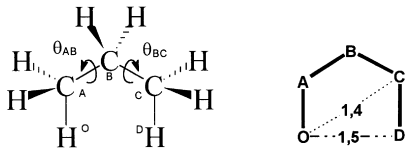

Scheme 11.

Eq. (50).

$$\begin{aligned}
&1,4\ \textit{separation} && \begin{cases} H^O \ldots C^C & (\textit{same as } C^C \ldots H^F) \\ C^A \ldots C^D & (\textit{same as } C^B \ldots H^F) \end{cases} \\
&1,5\ \textit{separation} && \begin{cases} H^O \ldots C^D & (\textit{same as } C^B \ldots H^F) \\ C^A \ldots C^E & \end{cases} \\
&1,6\ \textit{separation} && H^O \ldots C^E \\
&1,7\ \textit{separation} && H^O \ldots H^F
\end{aligned} \tag{50}$$

Fig. 14 shows, in accordance with and Scheme 13, that there are six different types of separation. Again, the two 1,4 separations in Fig. 11 are analogous to the $H^O \ldots H^C$ separation in ethane, the pair of 1,5 separations are analogous to the $H^O \ldots H^D$ separation in propane and the 1,6 separation is similar to the $H^O \ldots H^E$ separation in butane. Consequently, the pentane case may be regarded, at least topologically, as the 1,3 disubstituted propane or the 1-monosubstituted butane.

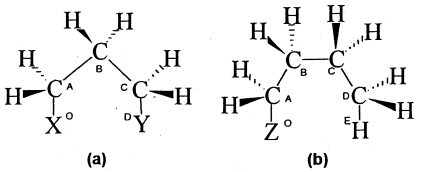

(51)

On the basis of the foregoing discussion (c.f. Figs. 10 and 13 as well as Eq. (48)), it is easy to conclude where the minimum and maximum

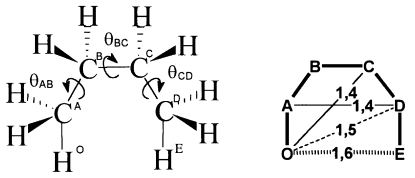

Scheme 12.

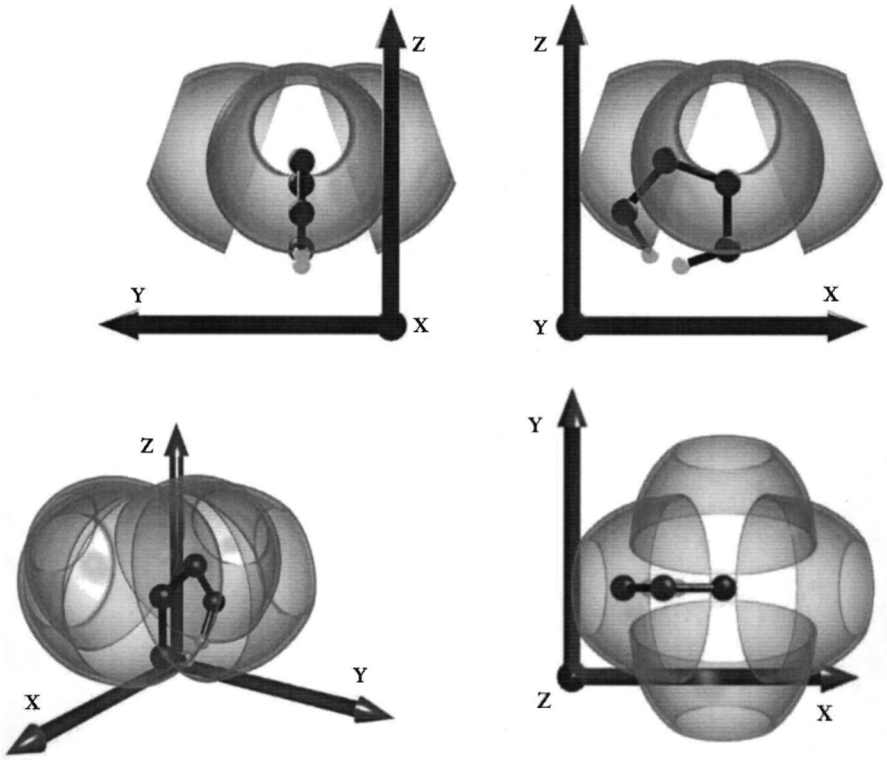

Fig. 11. Top, front side and perspective views of a partial illustration of the circular motions in butane involving the three torsional angles θ_{AB}, θ_{BC} and θ_{CD}.

separations are located Eq. (52) at the following torsional angles.

$$\text{minimum separation}: \quad \theta_{AB} = \theta_{BC} = \theta_{CD} = \theta_{DE} = 0^\circ \tag{52}$$

$$\text{maximum separation}: \quad \theta_{AB} = \theta_{BC} = \theta_{CD} = \theta_{DE} = 180^\circ$$

For the distance hypersurface of four independent variables Eq. (53) neither graphical presentation (like those of Figs. 3 and 6) nor topological representation (like Figs. 7 and 10) are possible

$$\left|\vec{R}_F\right| = f(\theta_{AB}, \theta_{BC}, \theta_{CD}, \theta_{DE}) \tag{53}$$

Viewing the structures in Schemes 10–13, it appears that separation of the terminal hydrogens are getting progressively closer to each other. The separation of these terminal hydrogen atoms, denoted as $|R_X|$, are summarized in Table 1. It does appear that a 'stereochemical catastrophe' is becoming inevitable in the case of pentane.

6. Multidimensional conformational analysis (MDCA)

In the previous section, internal rotations were assumed to be continuos in the sense that any confor-

Table 1
Minimal distance separation of terminal hydrogen atoms of straight chair hydrocarbons, C_nH_{2n+2}, where $2 \leq n \leq 5$, in their fully eclipsed conformation

Interaction	C_nH_{2n+2}	$\lvert\vec{R}_X\rvert$ (Å)
1,4	Ethane	2.260
1,5	Propane	1.927
1,6	Butane	0.886
1,7	Pentane	0.576

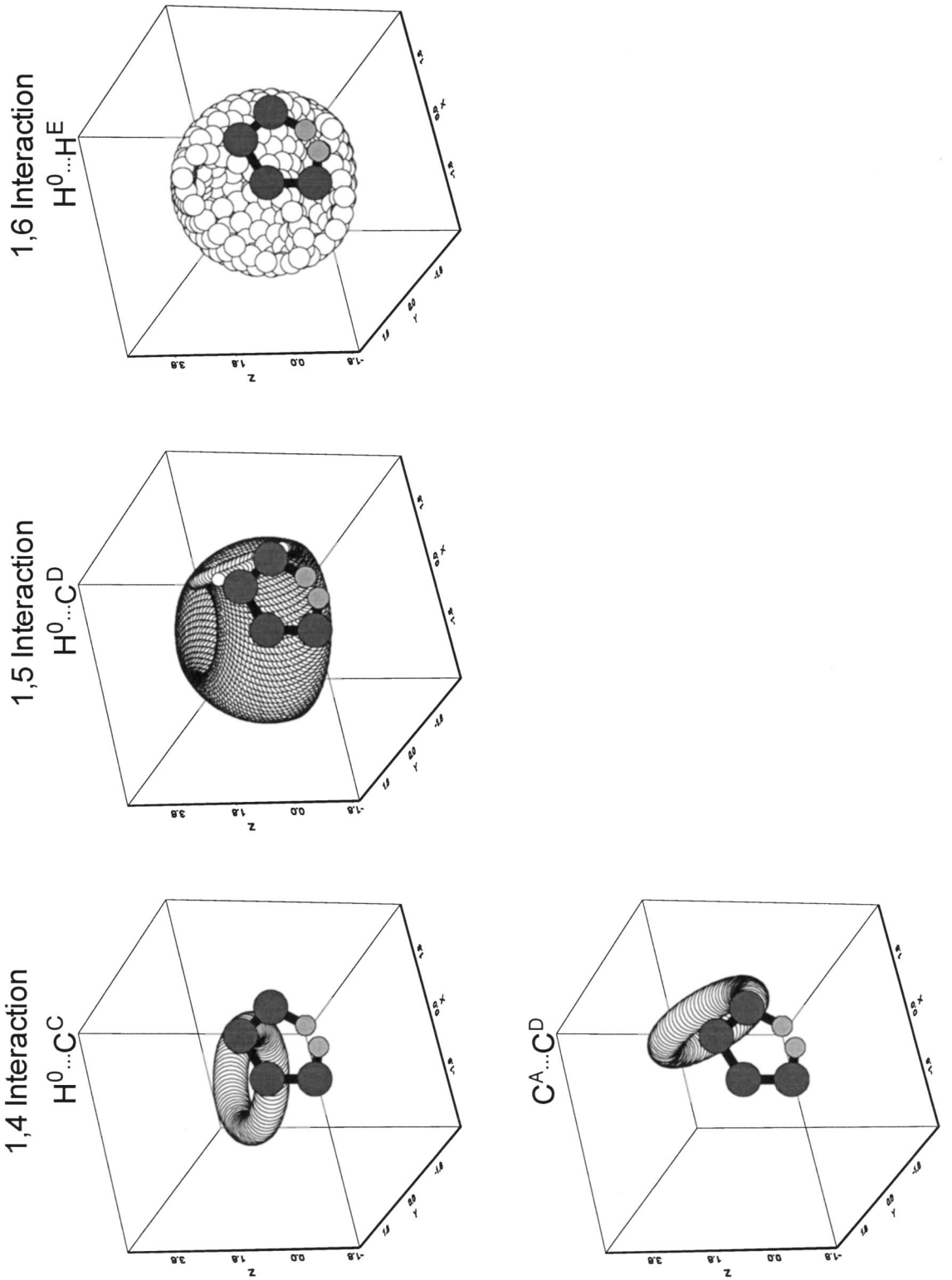

Fig. 12. Separation of the two terminal hydrogens (a 1,6 separation) in butane. Two 1,4 separations (H^O–C^C and C^A–C^D) and one 1,5 separation (H^O–C^D) are also shown for comparison.

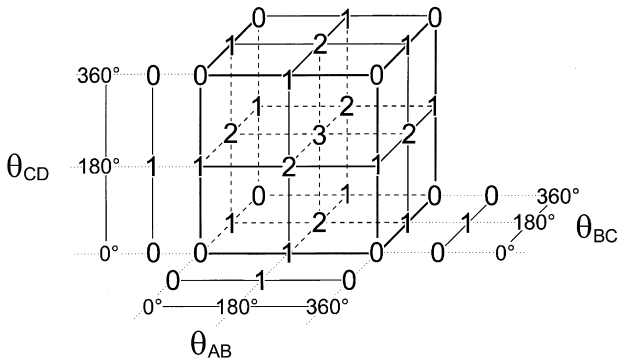

Fig. 13. Topology of the $|\vec{R}_E| = f(\theta_{AB}, \theta_{BC}, \theta_{CD})$ separation function [c.f Eq. (49)]. Critical points are denoted by their index: minimum is 0, first order saddle point is 1, second order saddle point is 2 and maximum is 3. Topologies of single rotations are denoted as 0–1–0 and are shown as a horizontal, diagonal and vertical lines at the bottom for θ_{AB}, at the right-hand side for θ_{BC} and at the left-hand side for θ_{CD}, respectively.

mation was regarded as an equally plausible structure. However, we know that even a single rotor may have only discrete conformers which we usually denote as *gauche*(+) or g^+, *anti* or *a* (sometimes denoted *t* for *s-trans*) and *gauche*(−) or g^- as illustrated in Fig. 15.

The previously presented circular motions for a single rotor (Fig. 4), for a double rotor (Fig. 7) and for a triple rotor (Fig. 11) associated with ethane, propane and butane, respectively, are shown again with some modification in Figs. 16–18, respectively. These Figs. show not only the circular motions for single, double and triple rotors, respectively, but they specify the location of the minima (g^+, *a*, g^-) by a small semi-transparent sphere. The location of the transition structures are also indicated by a cross. The graphical representation for a quadruple rotor (pentane) is not even attempted since the figure. depicting butane (a triple rotor) is already too crowded.

We are now in the position to reformulate the question of substituent proximity between terminal atoms or any other pair of atoms. The maximum separation between terminal atoms remains at $\theta = 180°$ since that torsional angle corresponds to the *a* conformer. However, the minimum separation has to be reinterpreted since $\theta = 0°$ is not a minimum energy structure. The two gauche conformers ($\theta = \pm 60°$), however, represent geometries in which the terminal atoms assume minimum separation. Further, the *syn* (i.e. $\theta = 0°$) geometry is a transition structure between g^+ and g^-.

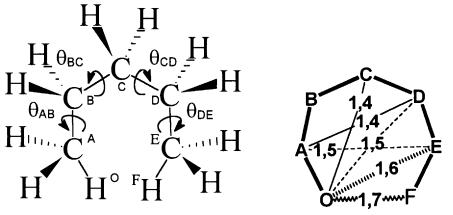

Scheme 13.

$$\begin{array}{ccccc} g^+ & \leftrightarrow & [syn]^{\neq} & \leftrightarrow g^- & \\ \theta = +60° & & \theta = 0° & & \theta = -60° \end{array} \quad (54)$$

Consequently, the previously determined minimum separation is characteristic to the *syn*-transition state.

In view of the foregoing discussion we may explore the following questions:

(a) What are the minimum and maximum separations between selected atom pairs (e.g. terminal hydrogens) *for stable conformations* of conformationally flexible molecules?
(b) What are the minimum and maximum separations between selected atom pairs (e.g. terminal hydrogens) *for transition conformations* of conformationally flexible molecules?

Ethane may be regarded as the trivial case (c.f. Scheme 10. Even though its rotation has three-fold periodicity (c.f. top curve of Fig. 19), the three minima are degenerate; there is only one unique minimum and one unique maximum corresponding to the

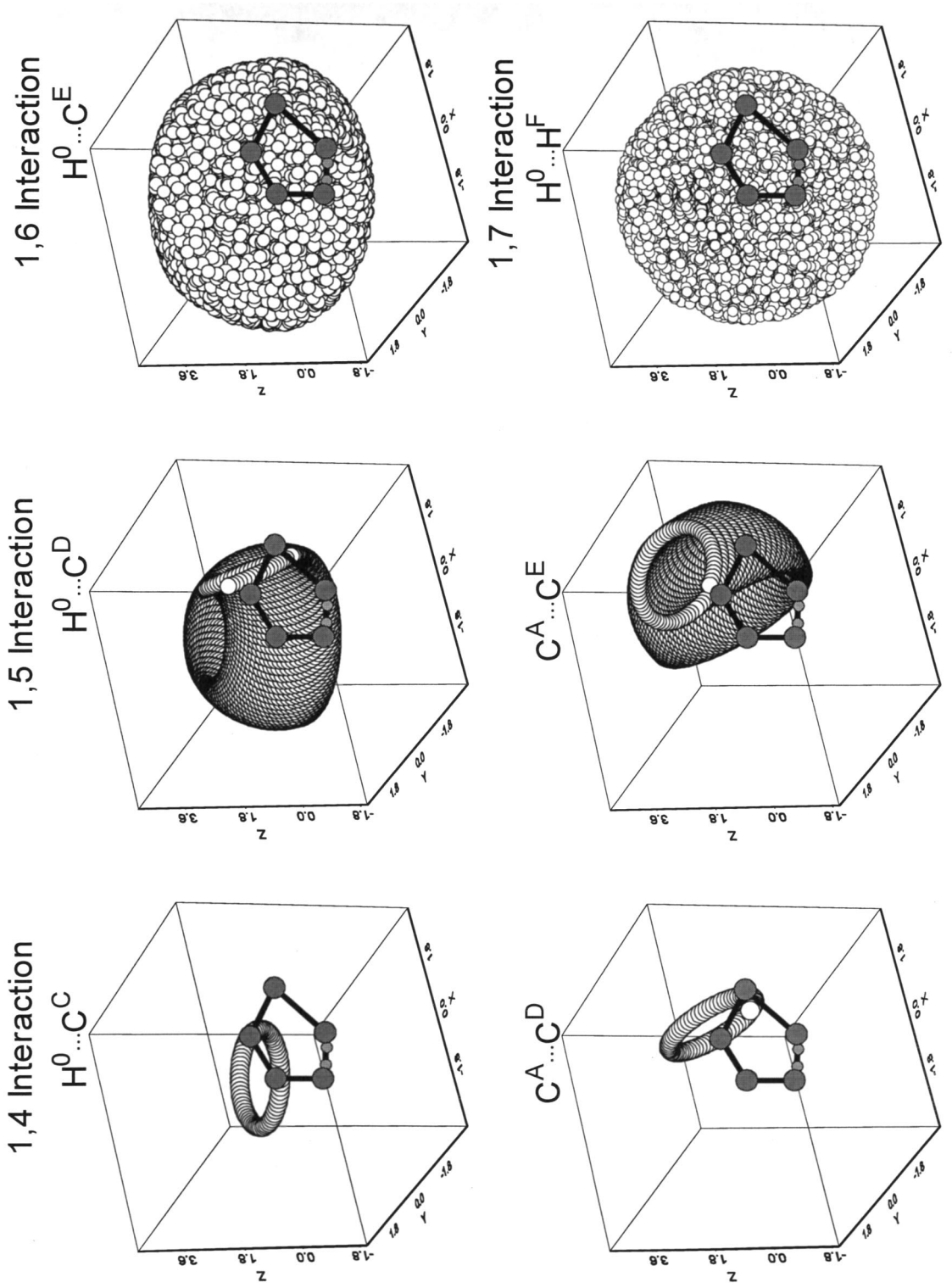

Fig. 14. Separation of the two terminal hydrogens (a 1,7 separation) in pentane. Two 1,4 separations (H^{O}–C^{C} and C^{A}–C^{D}) and two 1,5 separations (H^{O}–C^{D} and C^{A}–C^{E}) and one 1,6 separation (H^{O}–C^{E}) are also shown for comparison.

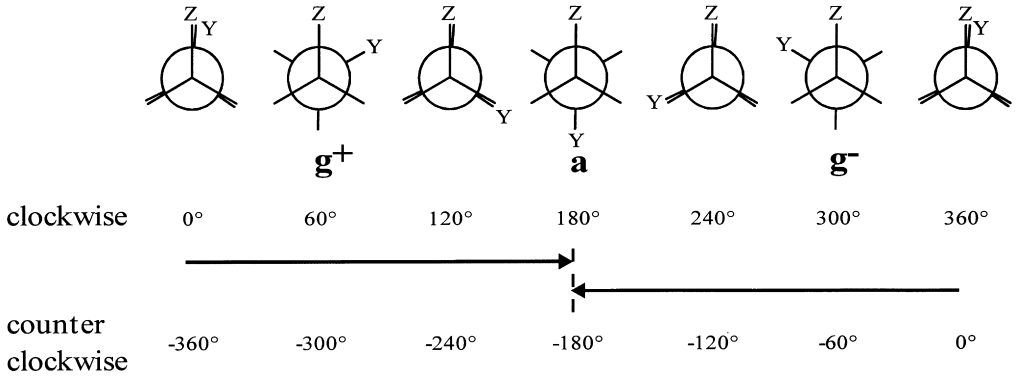

Fig. 15. Conformational changes of disubstituted ethane (Y–CH_2–CH_2–Z). The four C–H bonds are marked as four dashes, thus the presence of the H atoms is understood, but not shown explicitly (for ethane Y = Z = H, for *n*-butane Y = Z = CH_3).

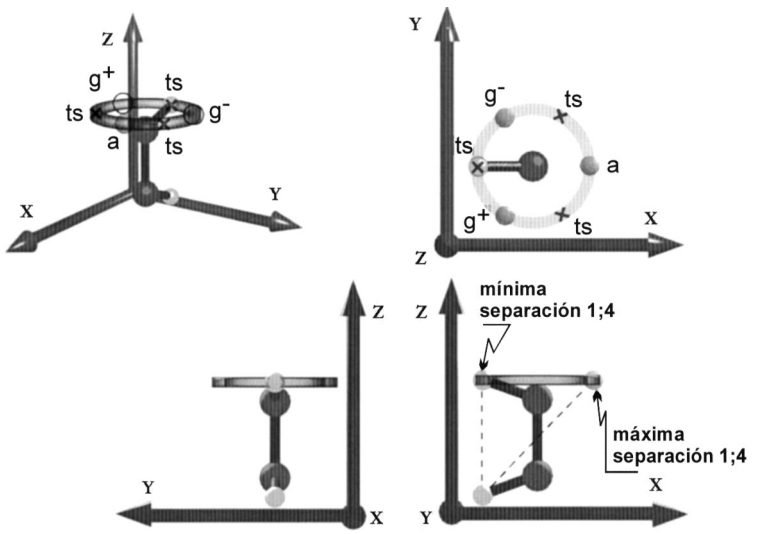

Fig. 16. Possible minima (g^+, *a*, g^- denoted by 0) and transition structure (ts, denoted by *X*) for a single rotor.

stable and transition conformations, respectively. The various unique distances between hydrogen atoms of the two methyl group are shown in Scheme 14.

Selected interatomic separations are shown in Table 2. It is clear from this table, as it might have been inferred from Scheme 14, that only two of the

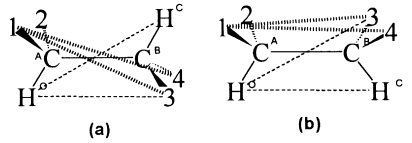

Scheme 14.

Table 2
Selected interatomic 1,4 separation for the stable ($\theta_{AB} = 180°$) and transition ($\theta_{AB} = 0°$) conformations of ethane using idealized geometry

d Atom pair	Separations (Å)[a] Stable conformation (Min. energy conformation)	Transition conformation (Max. energy conformation)
H^{O}–H^{3}	2.479	2.867
H^{O}–H^{C}	2.260	3.042
H^{1}–H^{3}	2.479	2.867
H^{1}–H^{4}	3.042	2.260

[a] Minimum and maximum separations are printed in bold for both the stable and the transition conformation.

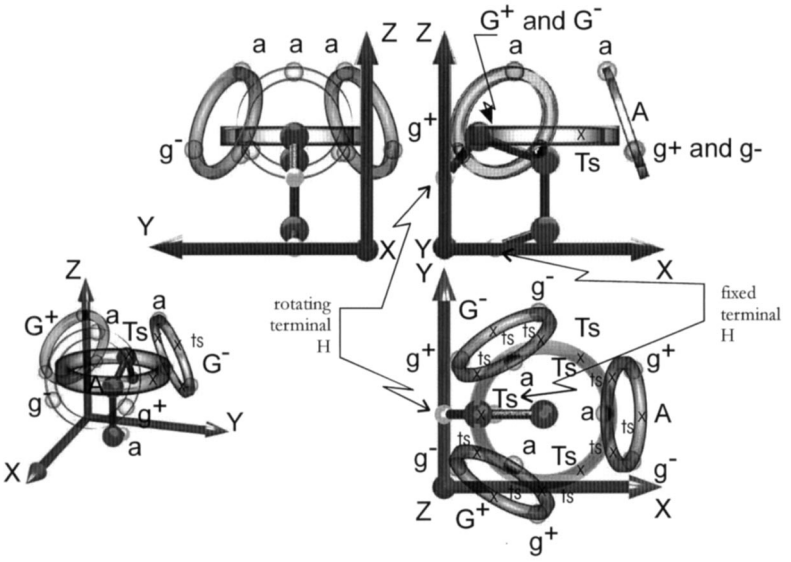

Fig. 17. Possible minima (g^+, a, g^- denoted by ○) and transition structure (ts, denoted by X) for a double rotor.

selected interatomic distances are unique. Thus we need to use only $H^0 \ldots H^3$ and $H^0 \ldots H^C$. Clearly, these distances may be denoted as 'long' and 'short' separation (c.f. Table 2), which is also illustrated in Fig. 19. This Fig. also shows, that the three-fold periodicity of the potential energy curve disappears in 1,2 disubstitution ($X–CH_2–CH_2–Y$). Also, note that the *syn* ($\theta_{AB} = 0°$) and the *anti* ($\theta_{AB} = 180°$) conformations are predetermined by symmetry even for 1,2 disubstituted ethane ($X–CH_2–CH_2–Y$). However, the location of the g^+ and g^-minima the g^+/a as well as a/g^- transition states are the results of the balance of stabilizing and destabilizing forces within the actual molecule.

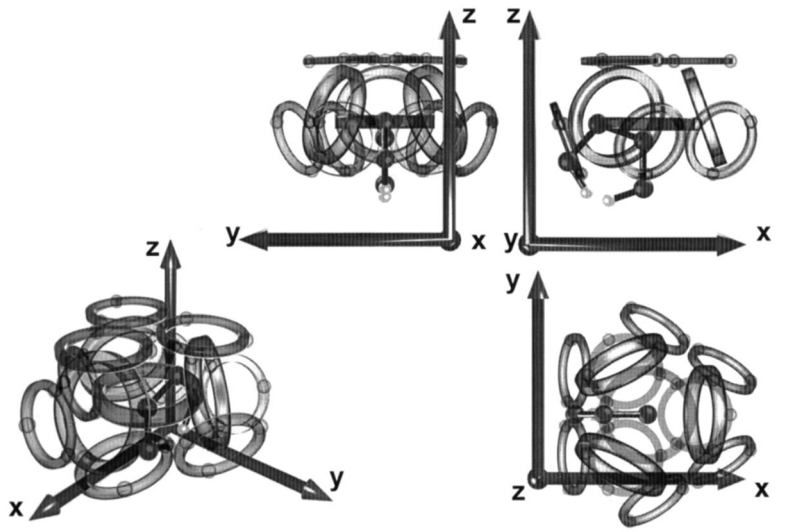

Fig. 18. Possible minima (g^+, a, g^- denoted by ○) for a triple rotor.

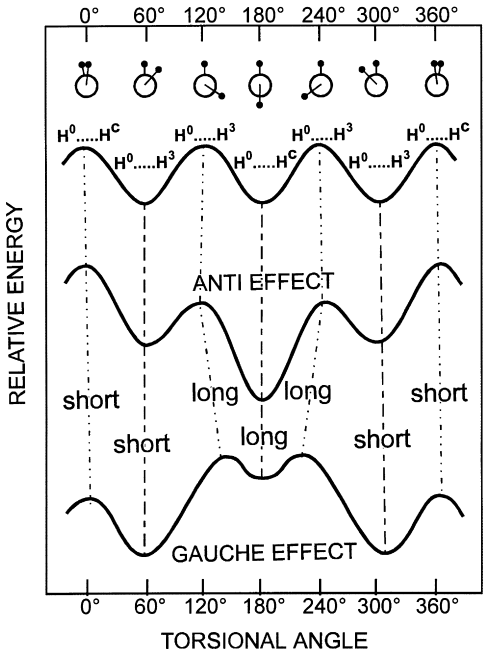

Fig. 19. Potential energy curves for ethane (top) and 1,2 disubstituted ethanes.

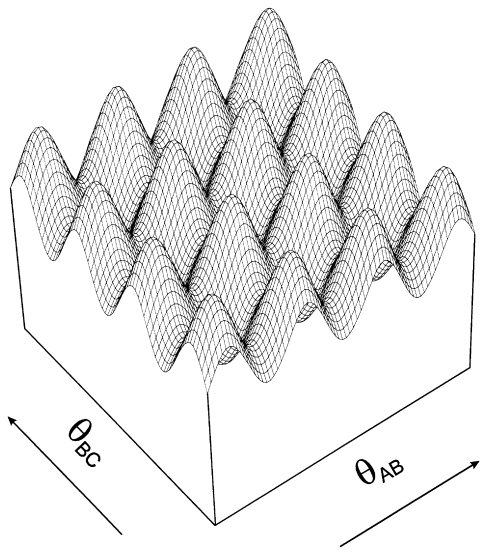

Fig. 20. Conformational potential energy surface (PES) of a double methyl rotor (e.g. propane). Full cycle of rotation (from 0° to 360°) is shown for both variables (θ_{AB} and θ_{BC}).

Propane looks like a trivial conformational problem with two equivalent torsional angle ($\theta_{AB}\theta_{BC}$), but the appearance is deceptive. Its potential energy surface (PES) is very monotonic due to the two equivalent rotating CH_3 groups (Fig. 20). The topology of the above surface is given in Fig. 21. The PES has nine minima but they are all equivalent. There is only one unique transition state which occurs 18 times and one unique maximum which is seen nine times on the surface. These three unique conformations are shown in Scheme 15. The 1,4 and 1,5 separations are summarized in Table 3.

It is clear that the minimum separation of $H^0 \ldots H^D$, calculated in the previous section is for the maximum ($\lambda = 2$) shown in Scheme 15c. Such proximity can never materialize because only minima ($\lambda = 0$) and transition structures ($\lambda = 1$) are visited during conformational change. However, the fully eclipsed structure ($\lambda = 2$ of Scheme 15c) is still a special structure corresponding to the (0,0) origin of the PES.

Monosubstitution at C^1 (c.f. Scheme 16) does alter the appearance of the PES (c.f. Fig. 22) implying that we do not have nine-fold degeneracy as it was the situation in the case of propane (c.f. Fig. 23). However, the topology of the two surfaces (Figs. 20 and 22) are the same having nine minima in both cases at the same general locations as illustrated in Fig. 23.

It is clear from Figs. 22 and 23 that there are only two and not three stable unique conformers of 1-fluoropropane because the g^+ and the g^- positions

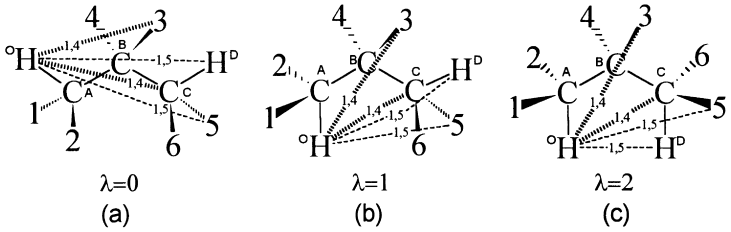

Scheme 15.

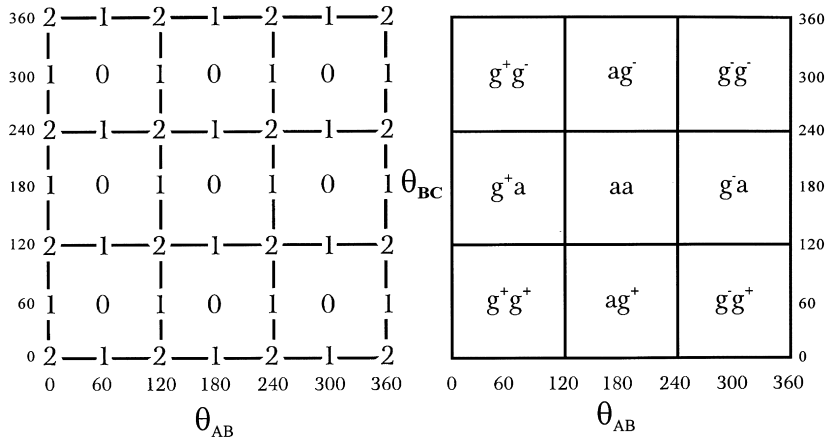

Fig. 21. Topology of the PES of propane. Left-hand side shows the index of the critical points (minimum, 0; transition structure, 1; and maximum, 2) Right-hand side shows the conformational assignment of the nine minima.

are equivalent. In one of the two conformers the F–C bond is anti to the C–C bond (denoted by circles in Fig. 23) and in the other one the F–C bond is *gauche* to the C–C bond (denoted by squares in Fig. 23). In the former case the number of distinctly different separations are the same as was in the case of the unsubstituted propane, only the numerical values are different (c.f. Table 4). However, in the latter case there is an increase in the number of unique separations since H^3 and H^4 became non-equivalent with respect to F in the *gauche* position. The same applies now for H^6 and H^7. The geometries and the unique separations of these two conformers are shown as the top structures in Scheme 16 while the actual values are summarized in Table 4.

As far as transition structures are concerned there are four such conformations denoted by roman numerals (*i–iv*). Two of them are along θ_{AB} and the other two are along θ_{BC} .

$$
\begin{aligned}
g^-g^+ &\rightarrow [i]^{\neq} \rightarrow g^+g^+ && (along\ \theta_{AB})\\
g^+g^+ &\rightarrow [ii]^{\neq} \rightarrow ag^+ \rightarrow [ii]^{\neq} \rightarrow g^-g^+ && (along\ \theta_{AB})\\
ag^+ &\rightarrow [iii]^{\neq} \rightarrow aa \rightarrow [iii]^{\neq} \rightarrow ag^- && (along\ \theta_{BC})\\
g^+g^+ &\rightarrow [iv]^{\neq} \rightarrow g^+a \rightarrow [iv]^{\neq} \rightarrow g^+g^- && (along\ \theta_{BC})
\end{aligned}
\tag{55}
$$

Table 3
Selected interatomic 1,4 and 1,5 separations for three unique conformations of propane with idealized geometry

Atom pair	Type of Interaction	Separation (Å)[a] Min. energy conformation ($\theta_{AB}=$ 180°, $\theta_{BC}=$ 180°)	Transition conformation ($\theta_{AB}=0°$, $\theta_{BC}=180°$)	Max. energy conformation ($\theta_{AB}=0°$, $\theta_{BC}=0°$)
$H^{O-}H^3$	1,4	2.479	2.867	2.867
$H^{O-}C^3$	1,4	3.453	2.452	2.452
$H^{O-}H^5$	1,5	3.724	2.425	3.197
$H^{O-}H^D$	1,5	4.278	3.520	1.927
$H^{1-}H^3$	1,4	3.042	2.260	2.260
$H^{1-}H^4$	1,4	2.867	2.479	2.867
$H^{1-}H^5$	1,5	2.515	3.665	3.690
$H^{1-}H^6$	1,5	3.072	3.212	4.090

[a] Minimum and maximum separations are printed in bold.

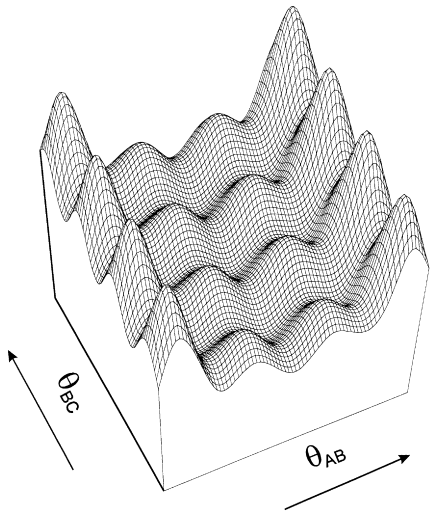

Fig. 22. Conformational PES landscape for monosubtituted propane molecule Z–CH_2–CH_2–CH_3 like 1-fluoropropane containing the pro-chiral central -CH_2- moiety. A full cycle of rotation (from 0° to 360°) is shown for both variables (θ_{AB} and θ_{BC}).

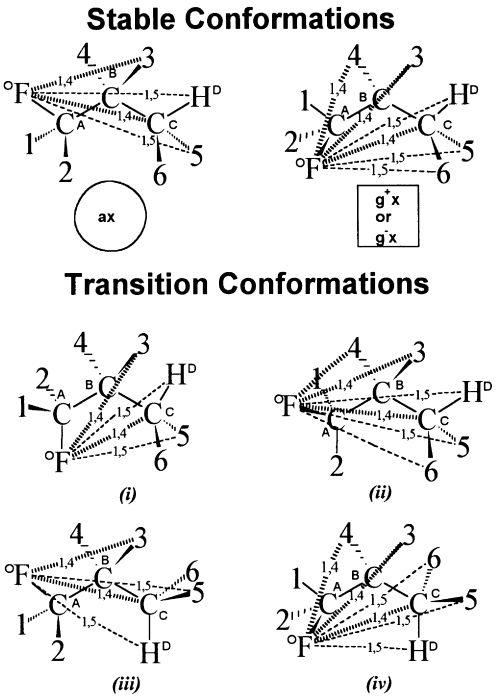

Scheme 16.

The location of these four unique transition states (*i–iv*) are clearly marked in Fig. 23B. The unique separations are also indicated graphically in Scheme 16 and their numerical values are summarized in Table 4. At the left-hand side the topology of the conformational PES of propane is also shown (c.f.

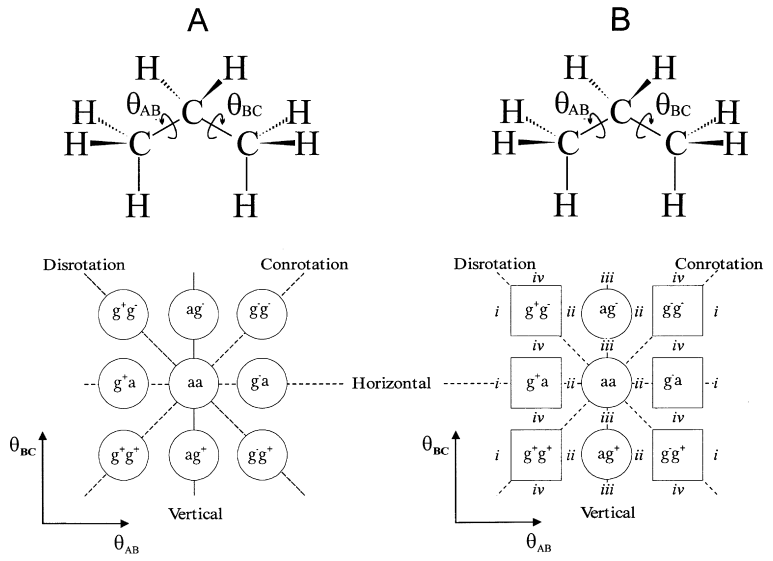

Fig. 23. A comparison of the conformational PES topology of propane and 1-fluoropropane.

Table 4
Selected interatomic 1,4 and 1,5 separations (a) for two unique stable conformers (b) and four unique transition conformers (*i–iv*) of 1-fluoropropane with idealized geometry.

Part A (F–C bond is syn or anti to C–C bond)		Separation (Å)		
Atom pair	Type of interaction	ax[a] (min)	i (TS)	iii (TS)
F^{O}–H^{3}	1,4	2.612	3.062	2.612
F^{O}–C^{C}	1,4	3.682	2.504	3.682
F^{O}–H^{5}	1,5	3.960	2.417	4.317
F^{O}–H^{D}	1,5	4.485	3.582	3.768
H^{1}–H^{3}	1,4	3.092	2.260	3.042
H^{1}–H^{4}	1,4	2.479	2.867	2.479
H^{1}–H^{5}	1,5	2.514	3.664	3.664
H^{1}–H^{6}	1,5	3.071	3.071	3.212
H^{1}–H^{D}	1,5	3.724	3.724	2.425
Part B (F–C bond is other than syn or anti to C–C bond)		Separation (Å)		
		gx[a] (min)	ii (TS)	iv (TS)
F^{O}–H^{3}	1,4	2.612	2.612	2.355
F^{O}–C^{4}	1,4	3.264	3.264	3.062
F^{O}–H^{C}	1,4	2.845	2.845	3.425
F^{O}–H^{5}	1,5	3.196	3.801	4.277
F^{O}–H^{6}	1,5	2.527	2.487	3.890
F^{O}–H^{D}	1,5	3.823	3.259	3.362
H^{1}–H^{3}	1,4	2.479	2.479	2.867
H^{1}–H^{4}	1,4	2.479	2.479	2.260
H^{2}–H^{3}	1,4	3.042	3.042	2.867
H^{2}–H^{4}	1,4	2.479	2.479	2.867
H^{1}–H^{5}	1,5	3.724	4.102	4.102
H^{1}–H^{6}	1,5	3.724	3.520	3.212
H^{1}–H^{D}	1,5	4.278	4.102	3.664
H^{2}–H^{5}	1,5	2.515	3.212	3.520
H^{2}–H^{6}	1,5	3.072	2.425	2.425
H^{2}–H^{D}	1,5	3.724	3.664	2.425

[a] $ax = ag^{+}, aa, ag^{-}; g^{+}x = g^{-}x = gx; g^{+}x = g^{+}g^{+}, g^{+}a, g^{+}g^{-}; g^{-}x = g^{-}g^{+}, g^{-}a, g^{-}g^{-}$.

Fig. 23A). Comparing the right-hand side with the left-hand side it becomes clear what a single substitution does to a PES.

Disubstitution at C^1 and C^2 further complicates the situation. It should be recognized that as the result of 1,2-disubstitution C^2 becomes a stereo center. Consequently *R* and *S* enantiomers may be generated. These enantiomers are shown in their most stable conformations in Scheme 17.

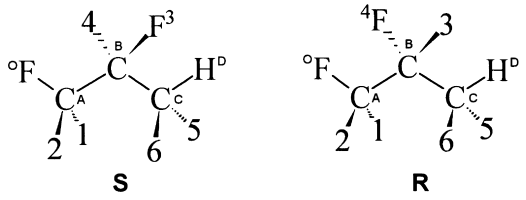

Scheme 17.

As a result of *R*, *S* enantiomerism, the analysis has to be done twice, once for the *R*- and for the *S*-enantiomer. However, the identification of the unique separations will be illustrated only once, for the *S*-enantiomer (c.f. Scheme 18). Nevertheless, the actual separations will be tabulated for both isomers. Tables 5 and 6 collect the data for the *S*-enantiomer and Tables 7 and 8 have the corresponding values for

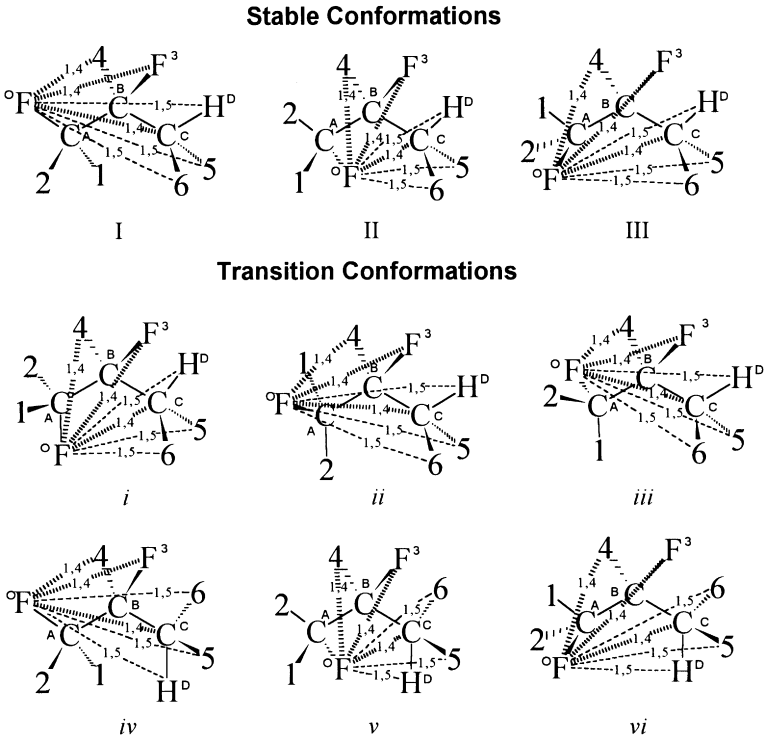

Scheme 18.

Table 5
Selected interatomic 1,4 and 1,5 separations for three unique stable conformers (g^+g^+, ag^+ and g^-g^-) of *S*-1,2 difluoropropane with idealized geometry

Atom pair	Type of interaction	Separation (Å) I (Min.)	II (Min.)	III (Min.)
F^O–F^3	1,4	2.732	2.732	3.490
F^O–H^4	1,4	3.264	2.612	2.612
F^O–C^C	1,4	2.845	3.682	2.845
F^O–H^5	1,5	3.196	3.960	2.527
F^O–H^6	1,5	2.527	3.960	3.200
F^O–H^D	1,5	3.828	4.485	3.828

Table 6
Selected interatomic 1,4 and 1,5 separations for six transition conformers (*i*–*vi*)

Atom pair	Type of interaction	Separation (Å) i (TS)	ii (TS)	iii (TS)	iv (TS)	v (TS)	vi (TS)
F^O–F^3	1,4	3.257	2.732	2.423	2.732	3.257	3.490
F^O–H^4	1,4	3.062	3.264	3.062	2.612	2.355	2.612
F^O–C^C	1,4	2.504	2.845	3.425	3.682	3.425	2.845
F^O–H^5	1,5	2.417	3.801	3.362	4.317	3.890	3.259
F^O–H^6	1,5	2.417	2.487	4.277	3.768	4.277	3.801
F^O–H^D	1,5	3.582	3.259	3.890	4.317	3.362	2.487

Table 7
Selected interatomic 1,4 and 1,5 separations for three unique stable conformers of *R*-1,2 difluoropropane with idealized geometry

Atom pair	Type of interaction	Separation (Å) I (Min.)	II (Min.)	III (Min.)
F^{O}–F^{3}	1,4	3.490	2.732	2.732
F^{O}–H^{4}	1,4	2.612	2.612	3.264
F^{O}–C^{C}	1,4	2.845	3.682	2.845
F^{O}–H^{5}	1,5	3.916	3.960	2.527
F^{O}–H^{6}	1,5	2.527	3.960	3.196
F^{O}–H^{D}	1,5	3.828	4.485	3.828

Table 8
Selected interatomic 1,4 and 1,5 separations for six transition conformers (*i–vi*)

Atom pair	Type of interaction	Separation (Å) i (TS)	ii (TS)	iii (TS)	iv (TS)	v (TS)	vi (TS)
F^{O}–F^{3}	1,4	3.257	3.490	3.257	2.732	2.427	2.732
F^{O}–H^{4}	1,4	3.062	2.612	2.355	2.612	3.062	3.264
F^{O}–C^{C}	1,4	2.504	2.845	3.425	3.682	3.425	2.845
F^{O}–H^{5}	1,5	2.417	3.801	3.362	4.317	3.890	2.487
F^{O}–H^{6}	1,5	2.417	2.487	4.277	3.368	4.277	3.801
F^{O}–H^{D}	1,5	3.582	3.259	3.890	4.317	3.362	3.259

the *R*-enantiomer. The numbers in the two tables reveal the non-superimposable mirror image relationship in the geometries of the *R*- and *S*-enantiomers.

The torsion about C^{A}–C^{B} leads to three different conformers (g^{+}, *a*, g^{-})because they are next to the chiral center. Thus one expects three distinctly different stable conformations.

Surface shown in Fig. 22 distorted about θ_{AB} with respect of the original three-fold periodicity. The F^{0}–C^{A} bond can also eclipse with three different bonds (C^{B}–C^{C}, C^{B}–F^{3} and C^{B}–H^{4}). This situation will lead to grand total of six unique transition conformations as shown below:

Torsion about C^{A}–C^{B}		Torsion about C^{B}–C^{C}		
3 eclipsed	×	1 staggered	3 transition conformations	(56)
3 staggered	×	1 eclipsed	3 transition conformations	

The three stable conformations and the six transition conformations are summarized in Scheme 18. This Scheme also shows the unique 1,4 and 1,5 separations.

The three unique minima are repeated three times so that there are nine minima on the conformational PES (c.f. Fig. 24A). Each of the six transition state are also repeated three times so all together are 18 transition states as required for an ideal conformational PES. All of these are summarized in Fig. 24A.

Disubstitution at C^{1} and C^{3} is somewhat simpler than the previous example since C^{2} is not a chiral centre. Note that to any symmetrically disubstituted propane (X–H_2–CH_2–CH_2–X) such as 1,3-difluoropropane may be regarded as a model for pentane in which the hydrogen atom of the two terminal CH_3 groups are ignored (c.f. Scheme 19)

Scheme 20 and Fig. 24B show all the expected stable (minimum energy) conformations. These nine stable conformations, however, encompass only four unique conformers. The degenerate conformations are denoted by circle, square and double square in Fig.

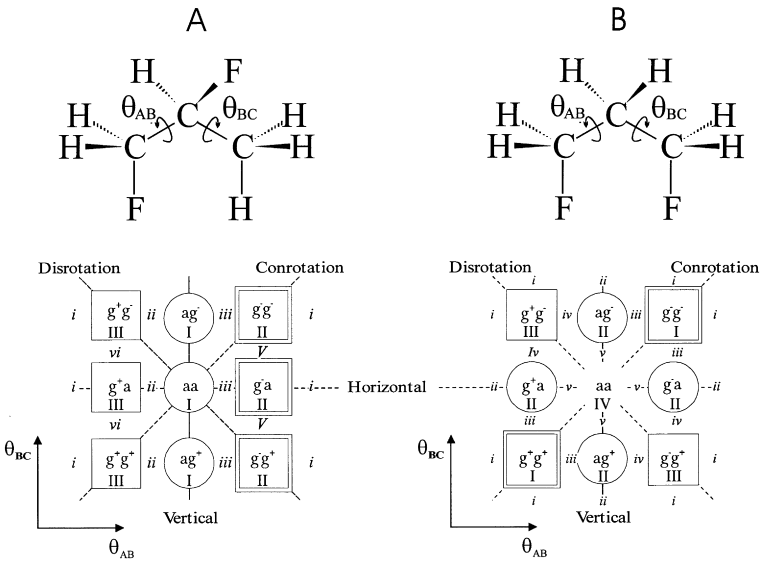

Fig. 24. Conformational PES topology of 1,3-disubstituted propane.

24B. The central (*a*, *a*) conformation is not duplicated on the surface. The four unique minima (I–IV) are accompanied by five (*i*–*v*) unique transition states these are also marked in Fig. 24B.

Selected 1,4 and 1,5 separations are shown for the four minima and the five transition states in Scheme 21. The calculated 1,4 and 1,5 distances are summarized in Tables 9 and 10.

6.1. Assessing numerical accuracy of GASCOS

The automatic generation of input files for force field or semi-empirical MO or *ab initio* molecular calculations within the framework of MCDA is one of the purposes of GASCOS. The other purpose is to give an early warning for any possible conformational catastrophy that may emerge on the conformational PES. This early warning can be obtained by searching for minimum distances among the conformers produced by GASCOS.

Take for example 1,3 difluoropropane. The following distances were predicted by GASCOS for the F…F distance for the conformers of the PES (c.f. Scheme 22).

This distance of 2.51 Å could possibly indicate a steric problem. While we may have anticipated this, on the basis of Scheme 22, as the two fluorine atoms are on the same side of the plane of the carbon skeleton, it is good to obtain a warning of this phenomenon.

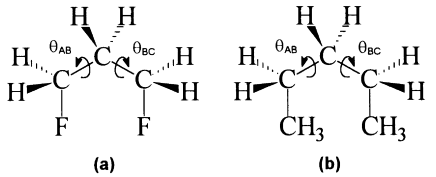

Scheme 19.

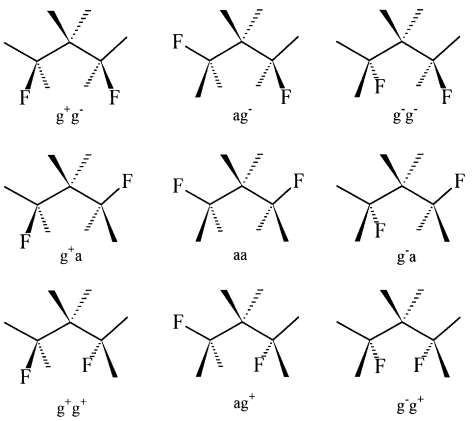

Scheme 20.

Stable Conformations

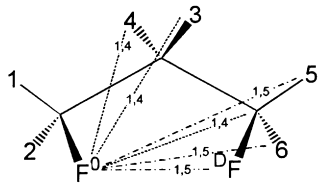

I

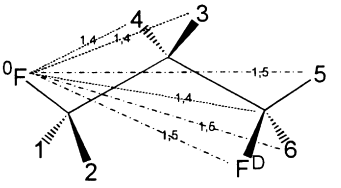

II

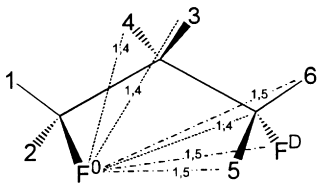

III

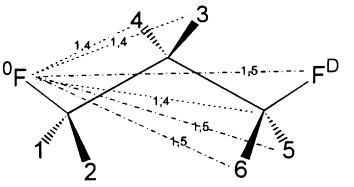

IV

Transitions Conformations

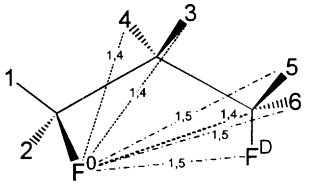

i

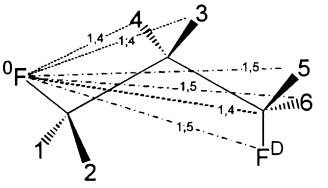

ii

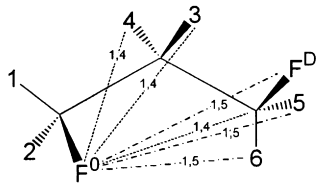

iii

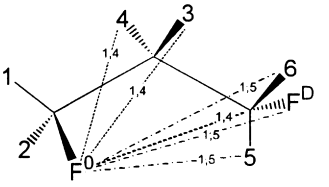

iv

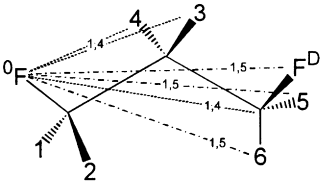

v

Scheme 21.

Table 9
Selected interatomic 1,4 and 1,5 separations for four unique stable conformers (g^+g^+, ag^+, g^-g^- and aa) of 1,3-difluoropropane with idealized geometry

Atom pair	Type of interaction	Separation (Å) I (Min.) g^+g^+	II (Min.) ag^+	III (Min.) g^-g^-	IV (Min.)ag^-
F^O–H^3	1,4	2.612	2.612	2.612	2.612
F^O–H^4	1,4	3.264	3.264	3.264	2.612
F^O–C^C	1,4	2.845	2.845	2.845	3.682
F^O–H^5	1,5	2.527	3.196	3.828	3.960
F^O–H^6	1,5	3.828	2.527	3.196	3.960
F^O–F^D	1,5	3.323	4.062	2.514	4.687

Table 10
Selected interatomic 1,4 and 1,5 separations for five transition conformers (*i–v*)

Atom pair	Type of.interaction	Separation (Å) i (TS)	ii (TS)	iii (TS)	iv (TS)	v (TS)
F^O–H^3	1,4	3.062	3.062	2.612	2.612	2.355
F^O–H^4	1,4	3.062	3.062	3.264	3.264	3.062
F^O–C^C	1,4	2.504	2.504	2.845	2.845	3.425
F^O–H^5	1,5	2.417	2.417	2.487	3.801	3.890
F^O–H^6	1,5	3.582	2.417	3.259	2.487	3.362
F^O–F^D	1,5	2.465	3.832	4.032	3.397	4.488

In the case of this small molecule we can actually see that the two F atoms are in each other's vicinity, however this may not be visible for a multidimensional problem.

The 2.51 Å is about 0.8 Å shorter than the nearest calculated F…F distance ($g^+g^+ = g^-g^- = 3.32$ Å). It would be nice to know if this is a false alarm due to the inaccuracy of the method or if it is for real. Also it would be nice to know if the calculated geometries

2.51 g^+g^-	4.06 $a\,g^-$	3.32 g^-g^-
4.06 g^+a	4.69 $a\,a$	4.06 $g^-\,a$
3.32 g^+g^+	4.06 $a\,g^+$	2.51 g^-g^+

Scheme 22.

may be regarded as acceptable starting points for ab initio computations.

In view of these considerations we carried out HF/6-31G computations on all the predicted minima of propane and the various fluoropropanes. Full geometry optimizations were performed on the following stable structures:

propane	1 minimum	(I)
1–fluoropropane	2 minima	(I–II)
[S]–1, 2–difluoropropane	3 minima	(I–III)
[R]–1, 2–difluoropropane	4 minima	(I–IV)
1, 3–difluoropropane	5 minima	(I–V)

The 1,4 and 1,5 separations of the optimized structures are presented, for the above five sets of compounds, in Tables 11–15, respectively.

The last column of each of these tables shows the deviation between the two methods of calculations:

$$\Delta D = D(GASCOS) - D(ab\ initio) \quad (57)$$

These values for the 1,4 separation ($\Delta D^{1,4}$) and the

Table 11
Idealized and optimized 1,4 and 1,5 separations of selected atomic pairs of the stable conformer of propane

Atom pair	Type of interaction	Separation (Å) Idealized conformation ($\theta_{AB} = 180°$, $\theta_{BC} = 180°$)	Optimized conformation ($\theta_{AB} = 180°$, $\theta_{BC} = 180°$)	Difference (Å)
$H^{O-}H^{3}$	1,4	2.479	2.491	− 0.012
$H^{O-}C^{C}$	1,4	3.453	3.494	− 0.041
$H^{O-}H^{5}$	1,5	3.724	3.804	− 0.080
$H^{O-}H^{D}$	1,5	4.278	4.326	− 0.048
$H^{1-}H^{3}$	1,4	3.042	3.058	− 0.016
$H^{1-}H^{4}$	1,4	2.479	2.511	− 0.032
$H^{1-}H^{5}$	1,5	2.515	2.633	− 0.118
$H^{1-}H^{6}$	1,5	3.072	3.164	− 0.092

Table 12
Idealized and optimized 1,4 and 1,5 separations of selected atomic pairs of the stable conformer of 1-fluorpropane

Atom pair	Type of interaction	Separation (Å) Idealized conformation	Optimized conformation	Difference (Å)
Part A I (ax)				
$F^{O-}H^{3}$	1,4	2.613	2.607	0.006
$F^{O-}C^{C}$	1,4	3.682	3.760	− 0.078
$F^{O-}H^{5}$	1,5	3.960	4.096	− 0.136
$F^{O-}H^{D}$	1,5	4.485	4.549	− 0.064
$H^{O-}H^{3}$	1,4	3.092	3.040	0.052
$H^{O-}H^{4}$	1,4	2.479	2.485	− 0.006
$H^{O-}H^{5}$	1,5	2.514	2.646	− 0.132
$H^{O-}H^{6}$	1,5	3.071	3.177	− 0.106
$H^{O-}H^{D}$	1,5	3.724	3.797	− 0.073
Part B II ($g^{+}x$ or $g^{-}x$)				
$F^{O-}H^{3}$	1,4	2.612	2.636	− 0.024
$F^{O-}H^{4}$	1,4	3.264	3.321	− 0.057
$F^{O-}C^{C}$	1,4	2.845	2.931	− 0.086
$F^{O-}H^{5}$	1,5	3.196	3.338	− 0.142
$F^{O-}H^{6}$	1,5	2.527	2.616	− 0.089
$F^{O-}H^{D}$	1,5	3.823	3.905	− 0.082
$H^{O-}H^{3}$	1,4	2.479	2.467	0.012
$H^{O-}H^{4}$	1,4	2.479	2.470	0.009
$H^{O-}H^{3}$	1,4	3.042	3.042	0.000
$H^{O-}H^{4}$	1,4	2.479	2.510	− 0.031
$H^{O-}H^{5}$	1,5	3.724	3.806	− 0.082
$H^{O-}H^{6}$	1,5	3.724	3.777	− 0.053
$H^{O-}H^{D}$	1,5	4.278	4.310	− 0.032
$H^{O-}H^{5}$	1,5	2.515	2.628	− 0.113
$H^{O-}H^{6}$	1,5	3.072	3.111	− 0.039
$H^{O-}H^{D}$	1,5	3.724	3.789	− 0.065

Table 13
Idealized and optimized 1,4 and 1,5 separations of selected atomic pairs of the stable conformer of *S*-1,2-difluoropropane

Atom pair	Type of interaction	Separation (Å) Idealized conformation	Optimized conformation	Difference (Å)
Part A I (g^+a)				
F^{O}–F^{3}	1,4	2.732	2.934	− 0.202
F^{O}–H^{4}	1,4	3.264	3.314	− 0.050
F^{O}–C^{C}	1,4	2.845	2.827	0.018
F^{O}–H^{5}	1,5	3.196	3.146	0.050
F^{O}–H^{6}	1,5	2.527	2.506	0.021
F^{O}–H^{D}	1,5	3.828	3.831	− 0.003
Part B III (g^-a)				
F^{O}–F	1,4	2.732	2.878	− 0.106
F^{O}–H^{4}	1,4	2.612	2.512	0.100
F^{O}–C^{C}	1,4	3.682	3.738	0.056
F^{O}–H^{5}	1,5	3.960	4.041	0.081
F^{O}–H^{6}	1,5	3.960	4.092	0.132
F^{O}–H^{D}	1,5	4.485	4.513	0.028
Part C II (aa)				
F^{O}–F^{3}	1,4	3.490	3.574	− 0.084
F^{O}–H^{4}	1,4	2.612	2.637	− 0.025
F^{O}–C^{C}	1,4	2.845	2.942	− 0.097
F^{O}–H^{5}	1,5	2.527	2.654	− 0.127
F^{O}–H^{6}	1,5	3.200	3.330	− 0.130
F^{O}–H^{D}	1,5	3.828	3.915	− 0.087

Table 14
Idealized and optimized 1,4 and 1,5 separations of selected atomic pairs of the stable conformer of *R*-1,2-difluoropropane

Atom pair	Type of interaction	Separation (Å) Idealized conformation	Optimized Conformation	Difference (Å)
Part A 1 (g^+a)				
F^{O}–F^{4}	1,4	3.490	3.574	− 0.084
F^{O}–H^{3}	1,4	2.612	2.637	− 0.025
F^{O}–C	1,4	2.845	2.942	− 0.097
F^{O}–H^{5}	1,5	3.200	3.330	− 0.130
F^{O}–H^{6}	1,5	2.527	2.654	− 0.127
F^{O}–H^{D}	1,5	3.828	3.915	− 0.087
Part B 111 (g^-a)				
F^{O}–F^{4}	1,4	2.732	2.878	− 0.146
F^{O}–H^{3}	1,4	2.612	2.512	0.100
F^{O}–C^{C}	1,4	3.682	3.738	− 0.056
F^{O}–H^{5}	1,5	3.960	4.092	− 0.132
F^{O}–H^{6}	1,5	3.960	4.041	− 0.081
F^{O}–H^{D}	1,5	4.485	4.513	− 0.028
Part C 11 (aa)				
F^{O}–F^{4}	1,4	2.732	2.934	− 0.202
F^{O}–H^{3}	1,4	3.264	3.314	− 0.050
F^{O}–C^{C}	1,4	2.845	2.827	0.018
F^{O}–H^{5}	1,5	2.527	2.506	0.021
F^{O}–H^{6}	1,5	3.196	3.146	0.050
F^{O}–H^{D}	1,5	3.828	3.831	− 0.003

Table 15
Idealized and optimized 1,4 and 1,5 separations of selected atomic pairs of the stable conformer of 1,3-difluoropropane.

Atom pair	Type of interaction	Separation (Å) Idealized conformation	Optimized Conformation	Difference (Å)
Part A I (g^+g^+)				
F^{O}–H^{3}	1,4	2.612	2.609	0.003
F^{O}–H^{4}	1,4	3.264	3.317	− 0.053
F^{O}–C^{C}	1,4	2.845	2.911	− 0.066
F^{O}–H^{5}	1,5	2.527	2.583	− 0.056
F^{O}–H^{6}	1,5	3.828	3.883	− 0.055
F^{O}–F^{D}	1,5	3.323	3.517	− 0.194
Part B II (ag^+)				
F^{O}–H^{3}	1,4	2.612	2.667	− 0.055
F^{O}–H^{4}	1,4	3.264	3.323	− 0.059
F^{O}–C^{C}	1,4	2.845	2.871	− 0.026
F^{O}–H^{5}	1,5	3.196	3.248	− 0.052
F^{O}–H^{6}	1,5	2.527	2.616	− 0.089
F^{O}–F^{D}	1,5	4.062	4.181	− 0.119
Part C III (g^+g^-)				
F^{O}–H^{3}	1,4	2.612	2.601	0.011
F^{O}–H^{4}	1,4	3.264	3.319	− 0.055
F^{O}–C^{C}	1,4	2.845	3.068	− 0.223
F^{O}–H^{5}	1,5	3.828	4.055	− 0.227
F^{O}–H^{6}	1,5	3.196	3.382	− 0.186
F^{O}–F^{D}	1,5	2.514	2.896	− 0.382
Part D IV (aa)				
F^{O}–H^{3}	1,4	2.612	2.607	0.003
F^{O}–H^{4}	1,4	2.612	2.607	0.003
F^{O}–C^{C}	1,4	3.682	3.738	− 0.056
F^{O}–H^{5}	1,5	3.960	4.100	− 0.140
F^{O}–H^{6}	1,5	3.960	4.100	− 0.140
F^{O}–F^{D}	1,5	4.687	4.756	− 0.069

Table 16
Ranges of derivation of 1,4 and 1,5 separations in propane and various flouropropanes

Compound	Min.	Ranges of $\|\Delta D^{1,4}\|$		Ranges of $\|\Delta D^{1,5}\|$	
		Min.	Max.	Min.	Max.
Propane	I	0.01	0.05	0.04	0.12
1-Fluoropropane	I	0.00	0.08	0.08	0.14
	II	0.00	0.09	0.03	0.15
[S]-1,2-difluoropropane	I	0.00	0.20	0.00	0.05
	II	0.06	0.15	0.02	0.14
	III	0.08	0.13	0.09	0.14
[R]-1,2-difluoropropane	I	0.02	0.10	0.09	0.14
	II	0.06	0.15	0.02	0.14
	III	0.05	0.20	0.00	0.06
1,3-Difluoropropane	I	0.00	0.07	0.06	0.19
	II	0.02	0.06	0.05	0.12
	III	0.05	0.22	0.18	0.38
	IV	0.00	0.06	0.06	0.15

1,5 separation ($\Delta D^{1,5}$) are summarized in Table 16 for all the structures studied.

It is interesting to note that at most of the times both $\Delta D^{1,4}$ and $\Delta D^{1,5}$ fell in the rang of 0.00 and 0.15 Å. These accuracies appeared to be satisfactory for input generation.

We had three cases where an $F^0 \ldots F$ distance in the GASCOS results, was in 'error' of 1.19 or 0.20 Å one case where the $F^0 \ldots H^6$ separation derivated by 0.18Å and one case where an $F^0 \ldots C^C$ distance showed a 0.22 Å discrepancy. The only alarming deviation was the $F^0 \ldots\ldots F^D$ separation (0.38 Å) in the g^+g (or its equivalent g^-g^+) conformation of 1,3-difluoropropane. The observed 0.38 Å was still considerably shorter than the approximately 0.8 Å difference between g^+g^-.(2.15 Å) and g^+g^+ (3.32 Å) conformations. Consequently, we can accept this as an early warning of a conformational catastrophe at the g^+g^- (or its equivalent g^-g^+) conformation.

It should be emphasised that the GASCOS method is performing rigid rotation; all bond lengths and bond angles are fixed. In contrast to that, the ab initio computations allow all parameters to be relaxed and this relaxation is causing the observed discrepancies in the ΔD values.

For examples in the case of 1,3-difluoropropane all bond angles varied within $\pm$ 3° of the tetrahedral value from 106.5° to 112.5°. The C–C–C bond angles were always among the larger values. However, the C–C–C bond angles for none of the conformations were as large as was for the g^+g^- orientation. (Scheme 23).

Structure	Conformation	∢CCC
I	g+g+	112.37
II	a g+	112.31
III	g-g+	**115.23**
IV	a a	112.17

Scheme 23.

Thus it appears that, with an excessive relaxation of the CCC bond angle, the system tried to avoid the conformational catastrophy in the g^-g^+ or g^+g^- conformations moving the two F atoms away from each other as much as possible.

7. Conclusions

Molecular conformations are partly geometry and partly electronics. For ideal molecular systems pure geometry dominates and electronic interactions simply follow; for non-ideal systems electronic interactions dominate and may override the geometrical factors. In view of the foregoing it seemed reasonable to code the pure geometrical factors which may be regarded as an appreciable component of multidimensional conformational analysis (MCDA).

The GASCOS (geometrical algorithm to search conformational space) program developed was able to asses the spatial requirement and, therefore, spatial proximity of rotating moieties within a given molecule. It also produced useful input-data for energy calculating programs (e.g. ab initio MO). In fact, GASCOS may be converted to be used as an automatic driver program for exploring multidimensional conformational space. Finally, the computed short distances which may occur in certain conformations may be used as early warning sings for possible conformational catastrophe that may emerge on a conformational PES.

Acknowledgements

The research was supported by grants from the Universidad Nacional de San Luis (UNSL) and the Consejo Nacional de Investigaciones Científicas y Técnicas (CONICET), Argentina. The continuous financial support of the Natural Sciences and Engineering Research Council (NSERC) is gratefully acknowledged.

References

[1] R.B. Silverman, The Organic Chemistry of Drug Design and Drug Actions, Academic Press, New York, 1992, p. 84.
[2] I.G. Csizmadia, Multidimensional theoretical stereochemistry and conformational potential energy surface topology, in: New Theoretical Concepts for Understanding Organic Reactions, Kluwer, Dordrecht, 1989, pp. 1–31.
[3] A. Perczel, R. Daudel, J.G. Angyan, I.G. Csizmadia, A study on the back-bone side-chain interaction in N-formyl-(L)-serine amide, Can. J. Chem. 68 (1990) 1882–1888.
[4] A. Perczel, J.G. Angyan, M. Kajtar, W. Viviani, J.-L. Rivail, J.F. Marcoccia, I.G. Csizmadia, Peptide models I. The topology of peptide conformational potential energy surfaces

(glycine and alanine derivatives), J. Am. Chem. Soc. 113 (1991) 6256–6265.
[5] A. Perczel, M. Kajtar, J.F. Marcoccia, I.G. Csizmadia, The utility of the 4D-Ramachandran map for the description of peptide conformations, J. Mol. Struct. 232 (1991) 291–319.
[6] W. Viviani, J.-L. Rivail, I.G. Csizmadia, Ab initio SCF calculations on conformations space of peptides models, Proceedings of the International Symposium on Advances in Biomolecular Simulations, OBERNAI (France), J. Chem. Phys. 88 (1991) 2505–2515.
[7] A. Perczel, W. Viviani and I.G. Csizmadia, Peptide conformational potential energy surfaces and their relevance to protein folding, in: J. Bertran (Ed.), Molecular Aspects of Biotechnology, Computational Models and Theories, Kluwer, Dordrecht, 1992, pp. 39–82.
[8] W. Viviani, J.-L. Rivail, I.G. Csizmadia, Peptide models II. Intramolecular interactions and stable conformations of glycine, alanine and valine peptide analogues, Theoret. Chim. Acta 85 (1992) 189–197.
[9] W. Viviani, J.-L. Rivail, A. Perczel, I.G. Csizmadia, Peptide models III. Conformational potential energy hypersurface of formyl-L-valine-amide, J. Am. Chem. Soc. 115 (1993) 8321–8329.
[10] A. Perczel, I.G. Csizmadia, A complete set of conformational elements defining secondary structures of proteins, J. Mol. Struct. (Theochem) 286 (1993) 75–85.
[11] C. Van Alsenoy, M. Cao, S. Newton, B. Teppen, A. Perczel, I.G. Csizmadia, F.A. Monramy, L. Schäfer, Conformational analysis and structural study by ab initio gradient geometry optimizations of the model tripeptide N-formyl-L-alanyl-L-alanine amide, J. Mol. Struct. (Theochem) 286 (1993) 149–163.
[12] M.A. McAllister, A. Perczel, P. Császár, W. Viviani, J.-L. Rivail, I.G. Csizmadia, Peptide models IV: topological features of molecular mechanics and ab-initio 2D-Ramachandran maps. A conformational data base for For-L-Ala-NH_2 and Ac-L-Ala-NH_2Me, J. Mol. Struct. (Theochem) 288 (1993) 161–180.
[13] M.A. McAllister, A. Perczel, P. Császár, I.G. Csizmadia, Peptide models V. Topological features of molecular mechanics and ab initio 4D-Ramachandran maps. A conformational data base for Ac-L-Ala-L-Ala-NHMe and for For-L-Ala-L-Ala-NH_2, J. Mol. Struct. (Theochem) 288 (1993) 181–198.
[14] A. Perczel, M.A. McAllister, P. Császár, I.G. Csizmadia, Peptide models VI: ab initio calculations on selected β-turn conformations predicted by ab initio calculations and confirmed by X-ray data of proteins, J. Am. Chem. Soc. 115 (1993) 4849–4858.
[15] G. Endrédi, C-M Liegener, M.A. McAllister, A. Perczel, J. Ladik, I.G. Csizmadia, The use of a modified Romberg formalism for the extrapolation of molecular properties from oliogmers to polymers — polyanine diamide in its ''extended-like'' or (γ_L)n or (C5)n conformation, J. Am. Chem. Soc. 115 (1993) 8275–8277.
[16] G. Endrédi, C-M. Liegner, M.A. McAllister, A. Perczel, J. Ladik, I.G. Csizmadia, Peptide models VIII. Folding energetics of the ''extended-like'' or (γ_L)n or (C5)n conformation of alanine oligopeptides, J. Mol. Struct. (Theochem) 306 (1994) 1–7.
[17] A. Perczel, M.A. McAllister, P. Császár, I.G. Csizmadia, Peptide models IX. A complete conformational set of For-Ala-Ala-NH_2 by ab initio computations, Can. J. Chem. 72 (1994) 2050–2070.
[18] M. Cheung, M.E. McGovern, T. Jin, D.C. Zhao, M.A. McAllister, A. Perczel, P. Császár, I.G. Csizmadia, Peptide models of proteins X. topological features of selected molecular mechanics and ab initio 6D-Ramachandran maps: a conformational data-base for For-L-Ala-L-Ala-L-Ala-NH_2 and Ac-L-Ala-L-Ala-L-Ala-NHMe, J. Mol. Struct. (Theochem) 309 (1994) 151–224.
[19] G. Endrédi, M.A. McAllister, A. Perczel, P. Császár, J. Ladik, I.G. Csizmadia, Peptide models VII. The ending of the right-handed helices in oligopeptides [For-$(Ala)_n$-NH_2 for $2 \leq n \leq 4$] and in proteins, J. Mol. Struct. (Theochem) 331 (1995) 5–10.
[20] G. Endrédi, M.A. McAllister, Ö. Farkas, A. Perczel, J. Ladik, I.G. Csizmadia, Peptide models XII. Topological features of molecular mechanics and ab initio 8D-Ramachandran maps: Conformational data for Ac-$(L\text{-}Ala)_4$-NHMe and For-(L-Ala)4-NH_2, J. Mol. Struct. (Theochem) 331 (1995) 11–26.
[21] Ö. Farkas, A. Perczel, J.F. Marcoccia, M. Hollósi, I.G. Csizmadia, Peptide models XIII. Side-chain conformational energy surface, $E = E(\chi,\chi^2)$ of N-formyl-L-serinamide (For-Ser-NH_2) in its γ_L or C_7eq backbone conformation, J. Mol. Struct. (Theochem) 331 (1995) 27–36.
[22] A. Perczel, Ö. Farkas, I.G. Csizmadia, Peptide models XVII. The role of the water molecule in peptide folding. An ab initio study on the right-handed helical conformations of N-formyl glycinamide and N-formyl-L-alaminamide monohydrates [H-(CONH-CHR-CONH)-H.H_2O; R = H or CH_3], J. Am. Chem. Soc. 117 (1995) 1653–1654.
[23] A. Perczel, I.G. Csizmadia, A search for the simplest structural units which are capable of describing the three-dimensional structure of proteins, Int. Rev. Phys. Chem. 14 (1995) 127–168.
[24] M.A. McAllister, G. Endrédi, W. Viviani, A. Perczel, P. Császár, J. Ladik, J.-L. Rivail, I.G. Csizmadia, Peptide models XI. Substitution effects on peptide chains. The magnitude of side-chain–backbone interactions in oligopeptides HCO-$(NHCHRCO)_4$-NH_2 for R = CH_3. An ab initio study, Can. J. Chem. 73 (1995) 1563–1572.
[25] P. Hudáky, A. Perczel, I.G. Csizmadia, Amino acid conformational analysis of proteins (ACAP), J. Mol. Struct. (Theochem) 362 (1996) 263–273.
[26] A. Perczel, Ö. Farkas, I.G. Csizmadia, Peptide models XVI. The identification of selected HCO-L-Ser-NH_2 conformers via a systematic grid search, using ab initio potential energy surfaces, J. Comp. Chem. 17 (1996) 821–834.
[27] A. Perczel, Ö. Farkas, I.G. Csizmadia, Peptide models XVIII. Hydroxymethyl side-chain induced backbone conformational shift of For-L-Ser-NH_2, J. Am. Chem. Soc. 118 (1996) 7809–7817.
[28] Ö. Farkas, M.A. McAllister, J.H. Ma, A. Perczel, M. Hollósi,

I.G. Csizmadia, Peptide models XIX. Side-chain conformational energy surface $E = f(\chi^1, \chi^2)$ and amide I vibrational frequencies of N-formyl-L-phenylalanine (For-Phe-NH_2) in its γ_L or γ^{inv} or C_7eq backbone conformation, J. Mol. Struct (Theochem) 369 (1996) 105–114.

[29] A. Perczel, Ö. Farkas, J.F. Marcoccia, I.G. Csizmadia, Peptide models XIV. An ab initio study on the role of side-chain–backbone interaction stabizing the building unit of right- and left-handed helices in peptides and proteins, Int. J. Quantum Chem. 61 (1997) 797–814.

[30] G. Endrédi, A. Perczel, Ö. Farkas, M.A. McAllister, G.I. Csonka, J. Ladik, I.G. Csizmadia, Peptide models XV. The effect of basis set size increase and electron correlation on selected minima of the ab initio 2D-Ramachandran map of For-L-Ala-NH_2, J. Mol. Struct. (Theochem) 391 (1997) 15–20.

[31] A. Perczel, Ö. Farkas, I.G. Csizmadia, Peptide models XX. Aromatic side-chain–backbone interaction is phenylalamine containing diamide model system. A systematic search for the identification of all the ab initio conformers of For-L-Phe-NH_2, Can. J. Chem. 75 (1997) 1120–1130.

[32] A.M. Rodriguez, H.A. Baldoni, F. Suvire, R. Nieto-Vasquez, G. Zamarbide, R.D.Enriz, Ö. Farkas, A. Perczel and I.G. Csizmadia, Characteristics of Ramachandran maps of alanine diamides as computed by various molecular mechanics, semi-empirical and Ab initio MO methods, J. Mol. Struct. (Theochem) 455 (1998) 275–301.

[33] A. Perczel, Ö. Farkas and I.G. Csizmadia, Peptide models XXI. Side-chain–backbone conformational interconversion in For-L-Ser-NH_2. Tracing relaxation paths by ab initio modeling, J. Mol. Struct. (Theochem) 455 (1998) 315–338.

[34] I. Jakli, A. Perczel, Ö. Farkas, M. Hollosi and I.G. Csizmadia, Peptide models XXII. A conformational model for aromatic amino acid residues in proteins. A conformational analysis of all the RHF/6-31 + G* conformers of For-L- Phe-NH_2, J.Mol.Struct. (Theochem) 455 (1998) 303–314.

[35] R. Haubner, R. Gratias, B. Diefenbach, S.L. Goodman, A. Jonczyk, H. Kessler, J. Am. Chem. Soc. 118 (1996) 7461.

[36] R. Haubner, W. Schmitt, G. Hölzemann, S.L. Goodman, A. Jonczyk, H. Kessler, J. Am. Chem. Soc. 118 (1996) 7881.

[37] M. Pfaff, K. Tangemann, B. Müller, M. Gurrath, G. Müller, H. Kessler, R. Timpf, J. Engel, J. Biol. Chem. 296 (1994) 20233.

[38] H.J. Bowen, M.A. Phil, J. Donohue, Tables of Interatomic Distances and Configuration in Molecules and Ions, Special Publication no. 11, The Chemical Society, London, 1958.

[39] M.R. Peterson, I.G. Csizmadia, J. Mol. Strct. (Theochem) 123 (1985) 399.

[40] Gaussian 94 (Revision D.1), M.J. Frish, G.W. Trucks, H.B. Schlegel, P.M. Gill, B.G. Johnson, M.A. Robb, J.R. Cheeseman, T.A. Keith, G.A. Peterson, J.A. Montgomery, K. Raghavachari, M.A. AlLaham, V.G Zakrzewski, J.V. Ortiz, J.B. Foresman, J. Defrees, J. Baker, J.P. Stewart, M. Head-Gordon, C. Gonzales and J.A. Pople, Gaussian, Inc., Pittsburg, PA, 1995.